Ocean Sci. Discuss., 3, 1011–1063, 2006
www.ocean-sci-discuss.net/3/1011/2006/

Ocean Science Discussions

Papers published in *Ocean Science Discussions* are under open-access review for the journal *Ocean Science*

Effects of mesoscale eddies on global ocean distributions of CFC-11, CO_2 and $\Delta^{14}C$

Z. Lachkar, J. C. Orr, J.-C. Dutay, and P. Delecluse

LSCE/IPSL, Laboratoire des Sciences du Climat et de l'Environnement, CEA-CNRS-UVSQ, Gif-sur-Yvette, France

Received: 19 June 2006 – Accepted: 19 July 2006 – Published: 31 July 2006

Correspondence to: Z. Lachkar (zouhair.lachkar@cea.fr)

Abstract

Global-scale tracer simulations are typically made at coarse resolution without explicitly modeling eddies. Here we ask what role do eddies play in ocean uptake, storage, and meridional transport of transient tracers. We made global anthropogenic transient-tracer simulations in non-eddying ($2^\circ \cos\varphi \times 2^\circ$, ORCA2) and eddying ($\frac{1}{2}^\circ \cos\varphi \times \frac{1}{2}^\circ$, ORCA05) versions of the ocean general circulation model OPA9. We focus on the Southern Ocean where tracer air-sea fluxes are largest. Eddies have little effect on global and regional bomb $\Delta^{14}C$ uptake and storage. Yet for anthropogenic CO_2 and CFC-11, increased eddy activity reduces southern extratropical uptake by 28% and 25% respectively. There is a similar decrease in corresponding inventories, which provides better agreement with observations. With higher resolution, eddies strengthen upper ocean vertical stratification and reduce excessive ventilation of intermediate waters by 20% between 60° S and 40° S. By weakening the Residual Circulation, i.e., the sum of Eulerian mean flow and the opposed eddy-induced flow, eddies reduce the supply of tracer-impoverished deep waters to the surface near the Antarctic divergence, thus reducing the air-sea tracer flux. Consequently, inventories for both CFC-11 and anthropogenic CO_2 decrease because their mixed layer concentrations in that region equilibrate with the atmosphere on relatively short time scales (15 days and 6 months, respectively); conversely, the slow air-sea equilibration of bomb $\Delta^{14}C$ of 6 years, gives surface waters little time to exchange with the atmosphere before they are subducted.

1 Introduction

The ocean's large capacity to take up and store carbon plays a major role in mediating the increase of anthropogenic CO_2 in the atmosphere. Therefore, accurately determining ocean uptake of anthropogenic tracers is relevant not only to understanding the global carbon cycle, but also to predicting the magnitude of future climate change. Ocean models have been used extensively to understand air-sea fluxes and ocean

OSD

3, 1011–1063, 2006

storage of anthropogenic carbon, which cannot be measured directly. During the last decade, the Ocean Carbon-Cycle Model Intercomparison Project (OCMIP) examined and compared several existing General Circulation Model (GCM) simulations of transient tracers (Orr et al., 2001; Dutay et al., 2002; Watson and Orr, 2003; Matsumoto et al., 2004). All the OCMIP models used a coarse-horizontal grid and resorted to parameterizing the effect of unresolved subgrid mixing processes on larger scales. The OCMIP models show a large disagreement in anthropogenic CO_2 air-sea flux within the southern extratropics (the region south of 20° S), which absorbs up to 50% of the global oceanic uptake (Orr et al., 2001; Watson and Orr, 2003). More recently, Matsumoto et al. (2004) compared simulated natural radiocarbon, anthropogenic CO_2, and CFC-11 from 19 ocean carbon cycle models with data-based estimates and also found large discrepancies between model results. These model discrepancies are partly associated with differences in the representation of subgrid-scale ocean mixing processes (Matear, 2001; Dutay et al., 2002). In the only attempt to date to use a global eddy resolving model (1/10°) to simulate the ocean CFC-11 distribution, Sasai et al. (2004) demonstrated much improved agreement with the observations in the southern extratropics. In particular, their model exhibits improved skill south of 40° S by limiting the excessive ventilation of thermocline and intermediate ocean that characterizes most of OCMIP coarse-resolution models. Thus, recent studies suggest that properly accounting for mesoscale eddies is one key to correctly simulate the uptake, transport, and storage of the transient tracers, especially in Southern Ocean. Additionally, to build a reliable eddy parameterization for coarse-resolution models, ocean modelers need to improve their understanding of how ocean eddies affect global and regional ocean tracer budgets.

During the past three decades, physical oceanographers have made significant advances in discerning the role that eddies play in the ocean's general circulation (Holland and Lin, 1975a,b; Holland, 1978). Cox (1985) investigated the effects of mesoscale eddies within the subtropical thermocline and highlighted the eddy-induced homogenization of anomalous Potential Vorticity along isopycnals. In terms of meridional

heat transport, Böning and Budich (1992) found a negligible effect of eddies when using a primitive equation model for an idealized ocean basin. Drijfhout (1994) showed that the eddy-induced mean meridional circulation nearly compensates poleward eddy heat transport for the case of a weak diabatic forcing. Vallis (2000) demonstrated how mesoscale eddies could be important in determining ocean stratification. Marshall et al. (2002) and Marshall and Radko (2003) used idealized simulations for a channel-only domain, finding that eddies help to set both the stratification and the depth of the permanent thermocline in the ocean.

Despite these advances, all studies have been limited by the compromises that must be made because of the computer-intensive nature of making simulations that include mesoscale variability in global-scale numerical models. Previous work has generally used simplified basin-scale models to investigate the genesis of mesoscale eddies and their interaction with the mean flow. Few studies indeed have addressed how ocean eddies may affect global-scale transport and distribution of transient tracers. Here we attempt to elucidate the importance of mesoscale eddies in terms of their effect on the global distributions of transient tracers. To isolate the effect of eddies, we follow the lead of Cox (1985) and Thompson et al. (1997), who compare integrations of a high-resolution and coarse-resolution versions of the same model.

In addition to anthropogenic CO_2, we also made simulations of CFC-11 and bomb $\Delta^{14}C$ to better evaluate model performance and to investigate how mesoscale eddies affect transient tracers with different air-sea equilibration times. That is, these three tracers require different times for their mixed-layer concentrations to equilibrate with the atmosphere. For a purely inert tracer, the equilibration time τ_{eq} can be estimated following (Broecker and Peng, 1974) as $\tau_{eq}=\frac{h}{v}$ where h is the mixed-layer depth and v the tracer piston velocity. Between 60° S and 40° S, the air-sea equilibration time for typical gaseous tracers, including CFC-11, is ~14 days, where as for bomb $\Delta^{14}C$ it is ~6 years. Lying between these two extremes is the anthropogenic CO_2's air-sea equilibration time of ~6-months. Equilibration for CO_2 is slower than for CFC-11 because when added to seawater, CO_2 does not remain a dissolved gas as does CFC-11; in-

OSD
3, 1011–1063, 2006

stead, it reacts with carbonate ion CO_3^{2-} to form bicarbonate ion HCO_3^-. What matters then is the change in the mixed-layer concentration of the sum of these three species (i.e., dissolved inorganic carbon DIC), not just the change in CO_2 concentration. Relative to CFC-11, the time for a perturbation in mixed-layer DIC to equilibrate with the atmosphere is longer by a factor of $\frac{\partial[DIC]}{\partial[CO_2*]}$ (Sarmiento and Gruber, 2006). That factor averages 12 between 60° S and 40° S whereas it averages 19 globally, based on the GLODAP data. For bomb $\Delta^{14}C$, the equilibration time between the mixed layer and the atmosphere is much longer still because isotopic equilibrium requires that CO_2 exchange its isotopic composition with the entire DIC pool. The correspondng factor is then $\frac{[DIC]}{[CO_2*]}$, which averages 140 between 60° S and 40° S and 180 globally.

The air-sea equilibration time has already been shown to affect transport and uptake of transient tracers in an idealized model of the Southern Ocean (Ito et al., 2004). Here we aim to use an ocean general circulation model (OGCM) to evaluate the effects of mesoscale eddies on large-scale uptake, storage and meridional transport of CFC-11, anthropogenic CO_2, and bomb $\Delta^{14}C$, while focusing particularly on the Southern latitudes where uptake is largest. We also aim to investigate how mesoscale eddies alter ocean dynamics in the higher southern latitudes and to examine the mechanisms by which they affect large-scale distributions of transient tracers.

2 Methods

2.1 Strategy

We made a series of simulations for CFC-11, anthropogenic CO_2 and bomb $\Delta^{14}C$, using a non-eddying version of the model having a $2^\circ \cos\varphi \times 2^\circ$ coarse-grid (termed ORCA2), where φ is latitude. We also made analogous simulations with an eddying version of the same model using a $\frac{1}{2}^\circ \cos\varphi \times \frac{1}{2}^\circ$ grid (ORCA05), whose grid size is 34 km on average, globally, and is 28 km at 60° S. The eddying version of the model

has sufficient horizontal resolution to resolve the largest mesoscale eddies (those with diameter larger than two or three times the grid size), although it leaves unresolved a large part of the mesoscale eddy spectrum. For comparison, to be fully "eddy-resolving" there would need to be at least 12 grid points per wavelength (Chassignet and Verron, 2006), i.e., a grid size at least six times smaller than the first Rossby Radius of deformation, which varies between 10 and 20 km in high latitudes (Chelton et al., 1998).

Despite this limitation, the eddying version of our model exhibits substantial eddy activity in the Southern Ocean along some of the most energetic currents in the world (Fig. 1); conversely, the coarse-resolution model exhibits no such activity. Here, we have deliberately avoided using any subgrid-scale eddy parameterization, in order to better capture the effect of resolving mesoscale eddies that goes along with an increase in horizontal resolution.

Integrating long global carbon simulations until near-steady state requires running the model for several thousands of years. At eddy-permitting resolution, that would extend far beyond presently available computing resources. To overcome this technical limitation, we used perturbation approaches for both anthropogenic CO_2 and bomb $\Delta^{14}C$. In so doing, we assume that the natural ocean carbon cycle is not affected directly by the anthopogenic perturbation. Thus we treat anthropogenic CO_2 and bomb $\Delta^{14}C$ as passive tracers excluding any possible response of the ocean biological process to the anthropogenic CO_2 increase. This approach was introduced for anthropogenic CO_2 by Siegenthaler and Joos (1992) and first used in a 3-D model by Sarmiento et al. (1992). Here we extend it to bomb $\Delta^{14}C$. Simulations of anthropogenic CO_2 begin on 1 January 1765 and are run until 1 January 2000 (industrial era); simulations for bomb $\Delta^{14}C$ start on 1 July 1954 and run until 1 January 2000 (nuclear era).

Despite the advantage of using a perturbation approach, realizing online global tracer simulations in an eddying, global-scale general circulation model of the ocean (OGCM) remains a challenge because it requires intense computational resources.

For example, a 235-year anthropogenic CO_2 simulation (1765–2000), with our eddying model, requires 11 000 CPU-hours on one processor of a NEC-SX6 vectorial supercomputer. To further reduce computational costs we used the offline approach for our tracer simulations. An offline model driven by monthly fields from an (online) eddy-permitting OGCM ($0.4^\circ \cos\varphi \times 0.4^\circ$) was used by Sen Gupta and England (2004) to investigate ventilation of the globally prominent water masses.

Hill et al. (2004) used a 1/6° North Atlantic regional model, finding that offline simulations remain faithful to online runs when the time-averaged flow fields are updated on a timescale shorter than 10 days. Here, we use a 5-day forcing frequency. With the non-eddying version of our model, the offline transient-tracer results closely resemble those obtained with the online version (see Fig. 2).

To evaluate simulations, we compared simulated to observed tracer distributions along vertical sections from the World Ocean Circulation Experiment (WOCE) and to gridded data products from Global Ocean Data Analysis Project (GLODAP). The GLODAP data consists of synthesized products from WOCE, the Joint Global Ocean Flux Study (JGOFS), and the Ocean Atmosphere Carbon Exchange Study (OACES) (Key et al., 2004).

2.2 Models

Our simulations were made with the ORCA-LIM global coupled ocean-sea ice model whose ocean component is based on version 9 of the model OPA (Océan PArallélisé, referred to as OPA9). OPA is a finite difference OGCM with a free surface and a non-linear equation of state following the Jackett and McDougall (1995) formulation (Madec and Imbard, 1996; Madec et al., 1998); The model has a contorted horizontal curvilinear mesh in order to overcome the North Pole singularity found in conventional grids. To avoid the typical northern singularity over the ocean, the OPA9 grid has two poles, one over Canada and the other over Asia, which allows for longer timesteps while still respecting the CFL stability criterion. Variables are distributed on C grid (Arakawa, 1972) on prescribed z- levels. The horizontal grid is also orthogonal and retains numerical

accuracy to the second order (Marti et al., 1992). The model is implemented on a Mercator grid, i.e., becoming finer at high latitudes following the cosine of latitude. With 46 levels in the vertical direction, the vertical grid spacing increases from 6 m at the surface to 250 m at the bottom. The bottom of the deepest level reaches 5750 m. Lateral tracer mixing occurs along isopycnal surfaces via Laplacian diffusion. We used horizontal viscosity with Laplacian and biharmonic formulation for the non-eddying and the eddying simulations, respectively. The biharmonic diffusion operator acts on smaller scales, admitting shorter wavelength structures on the mesh that the Laplacian would damp out by diffusion (Griffies et al., 2000). Vertical eddy diffusivity and viscosity coefficients are given by a second-order closure scheme based on a prognostic equation for the turbulent kinetic energy (TKE) (Gaspar et al., 1990; Blanke and Delecluse, 1993) and are enhanced in case of static instability. This TKE parametrization has been shown to improve the simulated equatorial dynamics and the thermocline in a high resolution model (Blanke and Delecluse, 1993). To advect temperature and salinity, we used the Total Variance Diminishing (TVD) advection scheme following Lévy et al. (2001).

The bathymetry is calculated using the 2′ bathymetry file ETOPO2 from NGDC (National Geophysical Data Center) (Smith and Sandwell, 1997; Jakobsson et al., 2000), except for the zone south of 72° S where it was computed from the BEDMAP data (Lythe and Vaughan, 2001). OGCM output was stored as 5-day averages to avoid aliasing of high-frequency processes (Crosnier et al., 2001). Initial conditions for the temperature and salinity fields were taken from Levitus et al. (1998) for the low and middle latitudes and from the PHC2.1 climatology (Steele et al., 2001) for high latitudes. The model was started from rest, then spun up for 8 years with a climatological seasonal forcing with daily frequency as computed from the 1992–2000 NCEP/NCAR 10-m wind stress and 2-m air temperature data (Kalnay et al., 1996). Additionally, we used monthly climatologies of precipitation (Xie and Arkin, 1996), relative humidity (Trenberth et al., 1989), and total cloud cover (Berliand and Strokina, 1980). Surface heat fluxes and freshwater flux for ocean and sea-ice were calculated using the empirical bulk parameterisation proposed by Goose (1997).

OSD
3, 1011–1063, 2006

The sea ice component of ORCA-LIM is the Louvain-la-Neuve sea ice model (LIM), a dynamic-thermodynamic model specifically designed for climate studies. A full description of LIM is given by Fichefet and Maqueda (1997).

To study passive tracers, we used a tracer-transport (offline) version of OPA (OPA Tracer 8.5) driven by 5-day averages of fields of advection and vertical turbulent diffusion from the dynamic (online) model. As for active tracers (temperature and salinity), we used isopycnal Laplacian mixing with the same lateral diffusion coefficients as in the dynamic model. We employed the flux-corrected-transport advection scheme from Smolarkiewicz (1982, 1983); Smolarkiewicz and Clark (1986). This advection scheme is little diffusive and is positive definite, i.e., it ensures positive tracer concentrations.

2.3 Passive tracer boundary conditions

2.3.1 CFC-11

CFC-11 (chlorofluorocarbon-11) is a purely anthropogenic trace gas, whose atmospheric concentration has increased from zero since the 1930s. Once it enters the surface ocean via gas exchange, CFC-11 is chemically and biologically inert. Thus it serves as a passive conservative tracer and tracks circulation and mixing processes that occur over decadal timescales (Wallace and Lazier, 1988; Doney and Bullister, 1992). The oceanic concentrations of CFC-11 are measured with high precision. To model CFC-11 ocean uptake, we followed the protocols defined by OCMIP-2 (Dutay et al., 2002). That is, passive tracer fluxes at the air-sea interface were calculated according to the classical formulation of air-sea gas exchange

$$F_{CFC} = K_{CFC}(pCFC - \frac{C_s}{\alpha_{CFC}})(1 - I) \quad (1)$$

where K_{CFC} is the CFC-11 gas transfer coefficient (mol m^{-2} yr^{-1} µatm^{-1}), pCFC is the partial pressure of CFC-11 from the reconstructed atmospheric history (Walker et al., 2000), and C_s is the modeled sea surface tracer concentration. α_{CFC} is the CFC-11

solubility in the sea water (Warner and Weiss, 1985) which depends on temperature and salinity at the surface; I is the fractional sea ice cover, which varies between 0 and 1. K_{CFC} is calculated from solubility and 10-m NCEP wind speed using the Wanninkhof (1992) formulation of gas transfer velocity. Time and space variations of total air pressure are neglected.

2.3.2 Anthropogenic CO_2

For the anthropogenic CO_2 we used the same boundary conditions as developed for OCMIP-2. The air-sea CO_2 flux is determined as:

$$F_{CO_2} = K_{CO_2}(\delta pCO_{2a} - \delta pCO_{2o})(1 - I) \quad (2)$$

where K_{CO_2} is the CO_2 gas transfer coefficient in mol m^{-2} yr^{-1} ppm^{-1} calculated following Wanninkhof (1992), δpCO_{2a} and δpCO_{2o} are respectively the atmospheric and the oceanic perturbation of carbon in ppm. The atmospheric perturbation is defined by

$$\delta pCO_{2a} = pCO_{2a} - pCO_{2a,0} \quad (3)$$

where pCO_{2a} is the partial pressure of atmospheric CO_2 as prescribed from the Enting et al. (1994) spline fit to Siple ice core and Mauna Loa atmospheric CO_2 data for 1765.0 to 1990.0 and from the 12-month smoothed GLOBALVIEW-CO_2 (2003) Mauna Loa data for 1990.5 to 2000.0. The $pCO_{2a,0}$ term is set to 278 ppm, the partial pressure of CO_2 at the beginning of simulation (1765).

Unlike CFC-11, CO_2 is highly soluble in seawater and is hydrolyzed to form other inorganic carbon species, i.e., bicarbonate and carbonate ions. To model CO_2 then, we must carry the sum of all three dissolved inorganic species, i.e., DIC, and in the case of a perturbation approach, the model carries only the anthropogenic component (δDIC). Hence, at the surface, we need to convert between δDIC carried by the model and δpCO_{2o} that is needed to compute the air-sea flux according to Eq. (2).

OSD
3, 1011–1063, 2006

EGU

To do so, we follow the lead of Siegenthaler and Joos (1992) and Sarmiento et al. (1992). That is, we express the oceanic perturbation in the partial pressure of CO_2 (pCO_{2o}) in terms of the perturbation in dissolved inorganic carbon (δDIC)

$$\delta pCO_{2o} = \frac{z_0[\delta DIC + \delta DIC_{\text{corr}}]}{1 - z_1[\delta DIC + \delta DIC_{\text{corr}}]} - pCO_{2a,\text{corr}} \quad (4)$$

where z_0 and z_1 are coefficients that depend on temperature. Here though, we have added two correction factors, δDIC_{corr} and $pCO_{2a,\text{corr}}$, to take into account that the starting value of $pCO_{2a,0}$ is different from the reference $pCO_{2a,\text{ref}}$=280 ppm that Siegenthaler and Joos (1992) used when developing the perturbation approach. More details are offered in the appendix.

2.3.3 Bomb $\Delta^{14}C$

To model bomb $\Delta^{14}C$, we treated the $^{14}C/^{12}C$ ratio as a concentration and used the perturbation approach. Therefore we do not simulate processes causing fractionation (Toggweiler et al., 1989a,b), which induces a small simulation error (Joos et al., 1997). As with any perturbation approach, the simulation must begin with the ocean and atmosphere containing zero bomb $\Delta^{14}C$. Historical estimates of atmospheric $^{14}C/^{12}C$ are available for 3 latitudinal bands (90° S–20° S, 20° S–20° N, 20° N–90° N) from the compilation made for OCMIP-3 (I. Levin, personal communication; T. Naegler, personal communication). Our approach accounts for the anthropogenic perturbation in CO_2 atmospheric concentrations unlike Toggweiler et al. (1989b) who used the pre-industrial level for the atmospheric forcing. We force the 3-box atmosphere to maintain observed values of bomb $\Delta^{14}C$ that were shifted upward by subtracting off values from July 1954, which are negative due to the Suess effect. Bomb $\Delta^{14}C$ enters the ocean via air-sea exchange of CO_2. Radioactive decay is included but not important for the short simulations made here.

Following Orr et al. (2001), the air-sea bomb $\Delta^{14}C$ flux $F_{^{14}C}$ can be expressed as:

$$F_{^{14}C} = \mu(C_a - C_o)(1 - l) \quad (5)$$

where C_a is atmospheric bomb $\Delta^{14}C$ ratio, C_o is the simulated surface ocean ratio, and the CO_2 replenishment rate μ is given by

$$\mu = K_{CO_2} \frac{pCO_{2a}}{DIC} \quad (6)$$

where DIC is the surface ocean concentration of dissolved inorganic carbon (taken as 2.0 mol m^{-3} (Toggweiler et al., 1989a).

3 Results

To highlight the impact of mesoscale eddies on the global tracer distributions, we examined how refining horizontal resolution affects tracer simulations in terms of ocean uptake, storage, and northward transport.

3.1 Ocean uptake

Figure 3a shows the zonal integrals of the cumulative fluxes for the three tracers obtained using the coarse-resolution model. Cumulative fluxes are calculated as the time-integrated air-to-sea fluxes since the beginning of the simulations, and are normalized by dividing by the total global uptake for comparison. Although all three tracers exhibit maximum uptake between 40° S and 50° S, the relative amount that is taken up south of 20° S varies: 65% for CFC-11, 56% for anthropogenic CO_2, and 50% for bomb $\Delta^{14}C$. These dissimilarities are due to the differences between the three tracers in terms of their in air-sea equilibration times and solubilities. Figure 4 presents the corresponding cumulative flux maps for the three tracers normalized by dividing each by its mean concentration. Clearly oceanic uptake is not distributed evenly over the different basins. For example, Atlantic Ocean absorbs up to 39% of the total CFC-11 uptake, although it covers only 26% of the total ocean area. For the two anthropogenic carbon tracers, there are smaller contrasts in uptake between basins, with the relative contribution of the Atlantic Ocean shrinking to 30% for anthropogenic CO_2 and, 27% for bomb $\Delta^{14}C$.

The air-sea fluxes of the three tracers also differ in their responses to increasing horizontal resolution (Fig. 5). The bomb $\Delta^{14}C$ uptake is nearly unchanged, both regionally and globally. In contrast, CFC-11 and anthropogenic CO_2 air-sea fluxes decrease by 28% and 25% in the southern extratropics and 22% and 18% in the World Ocean. The reduction of the CFC-11 air-sea flux is largest in the Atlantic Ocean (>33%), moderate in the Indian (23%), and weakest in the Pacific (~10%). In contrast for anthropogenic CO_2, the decrease in the air-sea flux is nearly uniform across all basins (see Table 1). In both resolutions, the peak uptake for CFC-11 remains south of 58° S and that for bomb $\Delta^{14}C$ remains at 52° S; conversely, the peak uptake for anthropogenic CO_2 shifts from 57° S to 54° S with the increase in horizontal resolution (Fig. 5). Later we show that this shift for anthropogenic CO_2 also affects its northward transport through the activity of Southern Ocean eddies.

3.2 Inventories

Maps of the inventory, i.e., vertical column integral of the tracer concentration, provide a 2-D picture of the spatial distribution of tracer storage in the ocean. Figure 3b shows the normalized zonal integral inventories, for each tracer for the coarse-resolution model. More than 62% of the global inventory of CFC-11 is stored south of 20° S, whereas only 49% of total uptake of anthropogenic CO_2 and 47% of bomb $\Delta^{14}C$ are stored in this same region. That is, the relative contribution of southern extratropics to the total air-sea flux is larger for CFC-11 than for the two other tracers (Fig. 3a).

Maps of these quantities (Fig. 6) reveal that the highest specific inventories (i.e., mass per unit area) are found in the North Atlantic and between 30° S and 50° S. Although the Atlantic Ocean exhibits substantially higher specific inventories than do the other basins, contrast between basins for ocean storage of anthropogenic CO_2 and bomb $\Delta^{14}C$ is smaller.

The decrease in air-sea fluxes of CFC-11 and anthropogenic CO_2 that accompanies increased horizontal resolution leads to equivalent reductions in the global tracer inventories of these two tracers. Yet, this global decrease is not the same for the three

OSD
3, 1011–1063, 2006

basins (Table 2). For both tracers, reductions are greatest in the Indian Ocean, with inventories of CFC-11 and anthropogenic CO_2 decreasing by 37% and 25%, respectively. These inventory reductions are even stronger than those for the Atlantic, where the reduction in fluxes is the largest (see Table 1). That is, besides the CFC-11 flux decrease in the Indian basin (23%), there is weaker Atlantic-to-Indian tracer transport in the eddying version of the model. Two processes appear responsible for the change in the Atlantic-Indian inter-ocean exchange: (i) the increase of Indian-to-Atlantic transport associated with the Agulhas Current's mesoscale eddies, and (ii) the decrease of eastward transport due to the eddy activity in the Atlantic sector of the Antarctic Circumpolar Current (ACC). Thus, eddies play an important role in the inter-basin transport of transient tracers. Hence, one might also expect that they contribute to meridional transport of transient tracers.

3.3 Northward transport

To detail meridional or northward transport of a transient tracer, we first compute tracer divergence as the zonal integral of the difference between cumulative flux and column inventory. Positive divergence (Flux-Inventory) indicates areas of tracer export or loss, and negative divergence indicates areas of tracer gain. Both are due to meridional transport. The integral of the tracer divergence from south to north is the time-integrated northward transport from the beginning of simulation (Fig. 7).

For bomb $\Delta^{14}C$, the meridional distribution of the northward transport is nearly the same for the two versions of the model. With CFC-11, there is a decrease of equatorward transport in the Northern Hemisphere between 35° N and 40° N at the position of the central mid-latitutde jet, lying at the boundary between the subtropical and subpolar gyre and characterized by high eddy activity. In contrast, meridional transport of CFC-11 in the Southern Ocean changes little with improved horizontal resolution. For anthropogenic CO_2, the decrease of equatorward transport in response to increased horizontal resolution is a general feature that occurs in both the Southern and the Northern Hemispheres, between 60° S and 50° N. The maximum of anthropogenic CO_2 flux in

OSD
3, 1011–1063, 2006

the Southern Ocean in the high resolution simulation occurs at 54° S, within the core of the ACC (and particularly in the Indian Ocean), which is characterized by high eddy activity. We hypothesize that the relative amount of anthropogenic CO_2 transported southward by eddies may be larger than for the two other transient tracers. In addition, the ratio of the timescale of the surface tracer concentration anomalies (related to the Sea Surface Temperature anomalies) to the lifetime of mesoscale rings could alter the amount of the eddy-driven transport transport relative to that driven by the mean flow. Such was already suggested by Drijfhout (1994) for heat transport. Future work aimed at gaining more insight into the mechanisms that drive these contrasts willl require a more detailed study of how the mesoscale eddies interact with the mean flow in terms of meridional transport of transient tracers having different air-sea equilibration times.

3.4 Validation of simulations and improvements

We compared simulations to data in order to evaluate results and to assess if increased horizontal resolution offers much improvement. Although our analysis includes all three anthropogenic tracers, the focus is mostly in CFC-11, for which direct measurements are available.

3.4.1 CFC-11 simulations

Figure 8 compares the two model inventories to the GLODAP data-based product (Key et al., 2004) over the three ocean basins. Higher resolution offers substantial improvement, particularly in the Indian basin where the coarse-resolution model overestimates the CFC-11 inventory by 64% between 50° S and 30° S. Conversely, south of 50° S near the Antarctic divergence, both versions underestimate the observations, mainly due to poor representation of the mixed layer depth which is, on average, 150 to 200 m shallower than observed (Fig. 9). This model deficiency is associated with insufficient vertical mixing produced by the current version of TKE scheme in OPA model within the upper ocean of southern high latitudes. Despite this poor performance in the highest

southern latitudes, there is little impact on basin-integrated inventories, because discrepancies occur in a region with relatively weak storage and little surface area. The global CFC-11 inventory in the non-eddying model is 27% larger than that obtained by the eddying model, with the latter being close to observed estimates (Key et al., 2004; Willey et al., 2004) (see Table 3). Both of these gridded data products rely on the WOCE CFC-11 observations although they used different interpolation procedures. In addition, the global inventory of our eddying model is close to that of the global 1/10° eddy-resolving model of Sasai et al. (2004).

Simulated CFC-11 column inventories were also compared to observations along three sections in the Southern Ocean: AJAX along the Greenwich meridian in 1983 (Warner and Weiss, 1992), WOCE I9S along 115° E in the Indian Ocean (1994–1995), and WOCE P15 section along 170° W in the South Pacific in 1996 (Fig. 10). Once again, increased resolution improves results north of 50° S in all three sections. The non-eddying model overestimates observed CFC-11 inventories along all three sections, as do most of OCMIP coarse-resolution models which do not account for mesoscale processes (Dutay et al., 2002).

For greater detail south of 40° S where the ocean storage is largest and where OCMIP models differ most (Dutay et al., 2002), we studied the full-depth I9S section at 115° E (Fig. 11). Consistent with Fig. 10, vertical penetration of CFC-11 north of Subantarctic Front (SAF) near 50° S is more realistic in the eddying model. The vertical distribution in the non-eddying simulation is too diffusive and substantially overestimates the observed penetration. South of the ACC (55° S), both versions substantially underestimate tracer penetration.

3.4.2 Anthropogenic CO_2 and bomb $\Delta^{14}C$ simulations

Figure 12 shows the zonal integral of anthropogenic CO_2 inventories per basin for both simulations and for the GLODAP data-based estimate. The eddying model generally captures the magnitude and spatial pattern of the data, despite some disagreement in the tropical and subtropical Pacific Ocean as well as south of the SAF where it un-

derestimates the data-based estimates (Sabine et al., 2004). The mixed layer depth is simply too shallow in this region as already shown in Fig. 9. Our eddying model's global CO_2 inventory of 98 Pg C in 1994 falls within the range of data-based estimate of Key et al. (2004) and Sabine et al. (2004) (see Table 3). Concerning bomb $\Delta^{14}C$, we have already shown that increased horizontal resolution does not substantially alter the simulated air-sea fluxes (Fig. 5). Both versions of the model also simulate similar bomb $\Delta^{14}C$ inventories, which generally agree with GLODAP data-based estimate (see Table 3) as shown in Fig. 13. In short, including eddies in our simulations made substantial difference and improved results for both CFC-11 and anthropogenic CO_2, particularly in the southern extratropics. Next, we explore the mechanisms behind these improvements.

4 Discussion

For insight into how mesoscale eddies affect transient tracer distributions, we explored the main differences between the dynamics of the eddying and the non-eddying simulations.

4.1 Eddies and Southern Ocean stratification

The simulated mixed layer is generally shallower in the eddying model (Fig. 9). The largest differences are found in the Indian and Atlantic sectors of the southern extratropics between 40° S and 60° S, where the winter mixed layer in the eddying model is locally, 200 to 300 m shallower than in the non-eddying model. Between 40° and 50° S, the non-eddying model's winter mixed layer is also deeper than observed, particularly in the Indian Ocean (de Boyer Montégut et al., 2004). Including mesoscale eddies in the higher resolution simulation substantially reduces the spurious wintertime convection in Southern Ocean. This reduction of wintertime convection by mesoscale eddies is consistent with previous findings for the effect of Gent and McWilliams eddy parame-

terization (Gent and McWilliams, 1990; Gent et al., 1995) on the strength of wintertime convection in the Southern Ocean (Hirst and McDougall, 1996; England and Hirst, 1997). Because convection is governed by the water column stratification, we may anticipate that there are major changes in stratification between the two experiments. Indeed, increased resolution changes simulated subsurface density between 60° S and 40° S by flattening isopycnal surfaces. That flattening strengthens upper ocean stratification, and yields a more realistic vertical density structure in the Southern Ocean. More specifically, baroclinic mesoscale eddies serve to release Available Potential Energy (APE) of the mean flow in the form of Eddy Kinetic Energy (EKE), thereby reducing the baroclinic instability and ensuring a more stable stratification. Marshall et al. (2002) also showed with idealized numerical experiments that mesoscale eddies play a key role in setting up the stratification. By strengthening vertical stratification in the Southern Ocean, mesoscale eddies affect the rate at which the thermocline and intermediate ocean are ventilated as well as how water masses are transformed within the upper ocean. As a consequence of the flattening of density surfaces, the vertical penetration of CFC-11 and anthropogenic CO_2 are reduced in the eddying model (Fig. 14).

4.2 Ventilation and water mass transformation in the upper Southern Ocean

Higher resolution and thus the presence of mesoscale eddies reduce the excessive vertical penetration of simulated CFC-11 between 60° S and 40° S (Fig. 11). For example, between 55° S and 50° S, waters at 1000 m contain more than 2 pmol l^{-1} in the non-eddying model but only around 0.5 pmol l^{-1} in the eddying model (as in the observations). Most of CFC-11 that penetrates into subsurface waters south of 20° S is carried by Antarctic Intermediate Water (AAIW) as it subducts south of the SAF. This intermediate water is easily identified by its tongue of fresh water, with its salinity minimum of 34.2 and a mean potential density of ~27.2, that extends equatorward from the Antarctic Polar Front Zone (APFZ) to intermediate depths at subtropical latitudes. The AAIW's CFC-11 inventory (Fig. 15 reveals that it is the non-eddying model's excessive formation of that water mass that is largely responsible for its excessive penetration of

OSD
3, 1011–1063, 2006

CFC-11 as well as anthropogenic CO_2 in the upper waters of the southern extratropics. The non-eddying model overestimates the observed CFC-11 content of the AAIW in all the basins, particularly in the Atlantic and in the Indian sectors of the Southern Ocean, where the excess reaches more than a factor of two. With increased resolution, the CFC-11 inventory in the AAIW (between isopycnal surfaces 27.0 and 27.4) is reduced by 20% between 60° S and 40° S, while the total volume of this layer decreases by 33% between 50° S and 60° S and by 19% between 50° S and 40° S. Thus, the excessive ventilation of the Southern Ocean in the non-eddying model is linked to excessive AAIW formation rate, mostly south of 50° S.

To better understand the source of AAIW, the meridional circulation, and the water mass transformations that occur in upper waters between 40° S and 65° S, we calculated the isopycnal transport streamfunction in both the eddying and non-eddying versions of the model. Averaging along density instead of depth coordinates avoids the spurious large apparent diapycnal motion in the upper Southern Ocean known as the Deacon Cell (Döös and Webb, 1994). When the isopycnal streamfunction is given on neutral density surfaces, McIntosh and McDougall (1996) showed that it approximates the so-called Residual mean circulation, which is the sum (calculated in depth coordinates) of the Eulerian circulation and the eddy-induced flow (Andrews and McIntyre, 1976; Holton, 1981). Near the ocean surface, where eddies are most active, neutral surfaces are tangential to σ_0 potential density surfaces (McDougall, 1987). Thus, for simplicity, following the lead of (Döös and Webb, 1994) we computed the isopycnal streamfunction relative to the surface (σ_0), by projecting model output onto 72 evenly-spaced potential density layers ranging from 21 to 28 (Fig. 16).

The residual circulation in the upper ocean south of 40° S is reduced from 30 Sv in the non-eddying model to 20 Sv in the eddying model. This reduction is not spread homogeneously throughout the entire southern region. With increased resolution, upwelling of Lower Circumpolar Deep Water (LCDW, σ_0=27.6–27.8), which drives formation of AAIW near the Antarctic divergence near 60° S, decreases by more than 15 Sv. On the other hand, the conversion of Upper Circumpolar Deep Water (UCDW, 27.4–27.6) to

OSD
3, 1011–1063, 2006

AAIW between 45° S and 55° S increases by about 5 Sv. Most of the formation of AAIW in the eddying model results from UCDW conversion from below the annual maximum of the mixed layer depth, termed the bowl, which separates the subsurface ocean from the interior ocean (Marshall and Nurser, 1992). Consequently, these interior intermediate waters have no immediate contact with the atmosphere and are not ventilated directly. In contrast, in the non-eddying model, a large part of AAIW is formed near the surface in the mixed layer by upwelling of NADW/LCDW at 60° S . At the surface, these waters exchange heat and transient tracer content directly with the overlying atmosphere. Thus the non-eddying model's excessive upwelling of LCDW leads to the excessive ventilation of AAIW (Fig. 15). Figure 16 also reveals that the diapycnal flux diminishes considerably in the eddying model as the isopycnal overturning streamlines become more horizontal. Such is not surprising, given that eddies facilitate meridional circulation along the isopycnal surfaces (Hallberg and Gnanadesikan, 2001). Next, we detail how these eddy-induced changes in water mass transformation within the upper waters of Southern Ocean, are linked to the corresponding decreases in the air-sea fluxes of transient tracers.

4.3 Surface water saturation and residence time

Eddies act to weaken residual circulation in the upper Southern Ocean, which is equatorward at the surface. Thus they act to increase accumulation of tracer-rich surface waters between 60° S and 55° S. This accumulation increases surface water saturation for tracers whose equilibration times are relatively short (CFC-11 and anthropogenic CO_2), thereby decreasing the corresponding air-sea difference in partial pressures and reducing the air-sea tracer fluxes. For instance, the increase in surface water saturation with increased resolution is evident for CFC-11 in 1994 in the Atlantic Ocean (Fig. 17). On the other hand, because of bomb $\Delta^{14}C$'s slow air-sea equilibration time of ∼6 years, its surface concentrations has little time to react to the slowdown in the surface equatorward transport.

To illustrate this eddy-induced slowdown of the residual circulation south of 40° S, we

examined the Lagrangian trajectories of individual particles that were launched from under the mixed layer of the upwelling region south of the ACC. For this analysis, we relied on the Lagrangian diagnostic tool ARIANE (Blanke and Raynaud, 1997; see complete documentation of ARIANE on http://fraise.univ-brest.fr/~blanke/ariane/doc.html). Figure 18 shows 4-year trajectories of particles launched from just below the mixed layer in the Indian Ocean at 60° S between 140° E and 120° E. In the non-eddying model, water parcels upwell to the surface and are rapidly transported northward across the ACC, whereas in the eddying model they spend more time in the mixed layer before they are transported northward. Thus with higher resolution, there is a substantial increase in the residence time of water parcels at the surface in the region of the Southern Ocean where air-sea tracer fluxes are largest.

4.4 GM parameterization

To determine to what extent the GM parameterization properly represents the effect of mesoscale eddies on the CFC-11 distribution, we made two additional CFC-11 simulations including the GM parameterization at both eddying and non-eddying resolutions, GM coefficients of thickness diffusivity and isopycnal diffusivity in both simulations were set to 10^3 m^2 s^{-1}. Figure 19 shows globally integrated zonal CFC-11 inventory as given by all four simulations and by the GLODAP data product. Applying GM parameterization in the non-eddying version of the model does improve results, but not enough. The non-eddying model with GM still substantially overestimates the observed inventory, whereas the eddying model generally agrees regardless of whether the GM formulation is applied or not. The problem may be related to GM being an adiabatic parameterization. Close to boundaries, particularly near the ocean surface, it is known that eddy fluxes have an important diabatic component (Robbins et al., 2000; Price, 2001). Misrepresentation of eddy diapycnal behaviour in the mixed layer could well lead to spurious exchange between the upper mixed layer and ocean interior.

5 Summary and conclusions

The effect of mesoscale eddies on global distributions of CFC-11, anthropogenic CO_2 and bomb $\Delta^{14}C$ was investigated by comparing eddying and non-eddying versions of the same coupled ocean-sea ice model ORCA-LIM. Our aim was to evaluate how explicitly simulating eddies affects ocean uptake, storage, and meridional transport of three different anthropogenic tracers. Our focus was on the Southern Ocean, where air-sea fluxes and meridional transport of transient tracers are the largest.

Comparable simulations with eddying and non-eddying versions of the same model revealed a 22% decrease in the global ocean uptake for CFC-11 and a 18% decrease for that of anthropogenic CO_2. The largest discrepancies occur in the Atlantic and Indian sectors of the Southern Ocean. Conversely, eddies have little effect on global and regional bomb $\Delta^{14}C$ uptake. By comparing basin-integrated cumulative fluxes and inventories, we found that eddies affect inter-basin tracer exchange of CFC-11 and anthropogenic CO_2, substantially reducing Atlantic-to-Indian Ocean tracer transport. This decrease may be associated with both (1) the increase of westward transport by the Agulhas Current from the Indian to the Atlantic basins and (2) the decrease of eastward transport by the ACC. Both changes derive from the effect of mesoscale eddies. Model-data comparison reveals that increased horizontal resolution improved model performance.

Our second goal was to provide an improved understanding of the role of eddies in the high southern latitudes. We have shown that including mesoscale eddies results in stronger upper ocean stratification in that region as manifested by a thinner mixed layer and flattened density surfaces in the eddying simulation. Eddies act to reduce ventilation of the intermediate ocean by the AAIW, mainly in the Indian and Atlantic sectors of the Southern Ocean. By diagnosing the upper meridional circulation in the Southern Ocean within an isopycnal framework, we show that the decrease of AAIW formation rate in near-surface waters on the southern flank of ACC (60° S) leads to a weaker ventilation of the thermocline and intermediate ocean. Indeed, eddies consid-

OSD
3, 1011–1063, 2006

erably reduce the conversion of LCDW to AAIW (–15 Sv) near the surface in the region of Antarctic Divergence (60° S–55° S), while simultaneously increasing the conversion of UCDW to AAIW (+5 Sv) at intermediate depths between 55° S and 45° S.

Because eddies reduce upper meridional circulation (residual circulation) in the Southern Ocean, they also serve to increase surface water saturation of transient tracers, which results in a reduction in air-sea tracer fluxes. Lagrangian trajectory analysis of particles launched from just below the mixed layer at 60° S in the upwelling zone of the Indian sector of Southern Ocean visually demonstrates how higher resolution increases surface residence time between 60° S and 50° S where tracer air-sea fluxes are the largest.

Unlike CFC-11 and anthropogenic CO_2, bomb $\Delta^{14}C$ air-sea fluxes are insensitive to the eddy-induced slowdown in the upper meridional circulation. The long air-sea equilibration time of bomb $\Delta^{14}C$ offers little time for it to react, between the time when water masses are upwelled to the surface near the Antarctic Divergence and when they are subducted a few degrees to the north near the SAF. Although similarities exist between these anthropogenic tracers, their contrasting sensitivities to the mesoscale eddies reemphasize that we must be careful when trying to use findings from CFC-11 and bomb $\Delta^{14}C$ to make inferences about anthropogenic CO_2.

Although it remains to be seen if further increases in horizontal resolution will substantially alter ocean model estimates of anthropogenic CO_2 uptake, this study highlights the general need for higher resolution, or at least improved subgrid-scale mixing parameterizations, in the ocean component of coupled atmosphere-ocean-ice climate models and coupled climate-carbon models that are used to predict future climate change. The link between horizontal resolution and ventilation of intermediate waters suggests that model estimates of future perturbations to the ocean's decadal-scale heat uptake could change when ocean mesoscale eddies start to be resolved in the next generation of climate models.

OSD
3, 1011–1063, 2006

Appendix A

Oceanic carbon perturbation δpCO_{2o} calculation

The equations used here are based on the perturbation approach of Sarmiento et al. (1992). The oceanic perturbation δpCO_{2o} is defined as the change in CO_2 partial pressure in the ocean from the beginning of the simulation (pre-industrial level). The plot of $\frac{\delta pCO_{2o}}{\delta DIC}$ versus δpCO_{2o}, where δDIC is the concentration of dissolved inorganic carbon of the perturbation at the surface (in $\mu mol\,kg^{-1}$), reveals a linear relation for δpCO_{2o} ranging from 0 to 200 ppm. Thus, we can express simply the oceanic carbon perturbation as a function of δDIC by

$$\frac{\delta pCO_{2o}}{\delta DIC} = z_0 + z_1 \delta pCO_{2o} \quad \text{(A1)}$$

where z_0 and z_1 are seasonally varying coefficients depending on temperature T (in degrees Celsius) as in Sarmiento et al. (1995)

$$z_0 = 1.7561 - 0.031618 \times T + 0.0004444 \times T^2 \quad \text{(A2)}$$

$$z_1 = 0.004096 - 7.7086 \times 10^{-5} \times T + 6.10 \times 10^{-7} \times T^2 \quad \text{(A3)}$$

Rearranging Eq. (A1) and modifying to allow simulations to start at a different reference value than $pCO_{2a,ref}$=280 ppm used in the original Siegenthaler and Joos (1992) equation for the perturbation approach gives

$$\delta pCO_{2o} = \frac{z_0[\delta DIC + \delta DIC_{corr}]}{1 - z_1[\delta DIC + \delta DIC_{corr}]} - pCO_{2a,corr} \quad \text{(A4)}$$

with

$$\delta DIC_{corr} = \frac{pCO_{2a,corr}}{z_0 + z_1 \times pCO_{2a,corr}} \quad \text{(A5)}$$

and

$$pCO_{2a,\mathrm{corr}} = pCO_{2a,0} - pCO_{2a,\mathrm{ref}} = 278\,\mathrm{ppm} - 280\,\mathrm{ppm} \quad \text{(A6)}$$

Acknowledgements. We thank A.-M. Treguier and G. Madec for discussions. We also thank S. Raynaud for his technical advice for using ARIANE and the ESOPA group at LOCEAN for the general support, improvements, and maintenance of the ocean model OPA-ORCA. Support for this research has come from the French Commissariat à l'Energie Atomique (CEA) and the EU CARBOOCEAN Project (Contract no. 511176 [GOCE]). Computations were performed at CEA (CCRT) supercomputing center.

References

Andrews, D. and McIntyre, M.: Planetary waves in horizontal and vertical shear: The generalized Eliassen-Palm relation and the mean zonal acceleration, J. Atmos. Sci, 33, 2031–2048, 1976. 1029

Arakawa, A.: Design of the UCLA general circulation model, numerical simulation of weather and climate, Tech. Rep. 7, University of California, Dept. of Meteorology, 1972. 1017

Berliand, M. E. and Strokina, T.: Global distribution of the total amount of clouds (in Russian), Hydrometeorological Publishing House, Leningrad, Russia, 71 pp., 1980. 1018

Blanke, B. and Delecluse, P.: Low frequency variability of the tropical Atlantic ocean simulated by a general circulation model with two different mixed layer physics, J. Phys. Oceanogr., 23, 1363–1388, 1993. 1018

Blanke, B. and Raynaud, S.: Kinematics of the Pacific Equatorial Undercurrent: an Eulerian and Lagrangian approach from GCM results, J. Phys. Oceanogr., 27, 1038–1053, 1997. 1031

Böning, C. and Budich, R.: Eddy dynamics in a primitive equation model: Sensitivity to horizontal resolution and friction, J. Phys. Oceanogr., 22, 361–381, 1992. 1014

Broecker, W. S. and Peng, T.-H.: Gas exchange rates between air and sea, Tellus, 26, 21–35, 1974. 1014

Chassignet, E. P. and Verron, J.: Ocean Weather Forecasting: An Integrated View of Oceanography, Springer, 2006. 1016

Chelton, D. B., deSzoeke, R. A., Schlax, M. G., Naggar, K. E., and Siwertz, N.: Geographical

variability of the first-baroclinic Rossby radius of deformation, J. Phys. Oceanogr., 28, 433–460, 1998. 1016
Cox, M.: An eddy resolving model of the ventilated thermocline, J. Phys. Oceanogr., 15, 1312–1324, 1985. 1013, 1014
Crosnier, L., Barnier, B., and Tréguier, A.: Aliasing of inertial oscillations in the 1/6° Atlantic circulation Clipper model: impact on the mean merididional heat transport, Ocean Modelling, 3, 21–32, 2001. 1018
de Boyer Montégut, C., Madec, G., Fischer, A. S., Lazar, A., and Iudicone, D.: Mixed layer depth over the global ocean: an examination of profile data and a profile-based climatology, J. Geophys. Res., 109, C12003, doi:10.1029/2004JC002378, 2004. 1027, 1053
Doney, S. and Bullister, J.: A chlorofluorocarbon section in the eastern North Atlantic, Deep-Sea Res., 39, 1857-1883, 1992. 1019
Döös, K. and Webb, D. J.: The Deacon Cell and the other meridional cells in the Southern Ocean, J. Phys. Oceanogr., 24, 429–442, 1994. 1029
Drijfhout, S.: Heat transport by mesoscale eddies in an ocean circulation model, J. Phys. Oceanogr., 24, 353–369, 1994. 1014, 1025
Dutay, J.-C., Bullister, J., Doney, S. C., Orr, J. C., Najjar, R. G., Caldeira, K., Campin, J.-M., Drange, H., Follows, M., Gao, Y., Gruber, N., Hecht, M. W., Ishida, A., Joos, F., Lindsay, K., Madec, G., Maier-Reimer, E., Marshall, J. C., Matear, R., Monfray, P., Mouchet, A., Plattner, G. K., Sarmiento, J. L., Schlitzer, R., Slater, R. D., Totterdell, I. J., Weirig, M.-F., Yamanaka, Y., and Yool, A.: Evaluation of ocean model ventilation with CFC-11: Comparison of 13 global ocean models, Ocean Modelling, 4, 89–120, 2002. 1013, 1019, 1026
England, M. H. and Hirst, A. C.: Chlorofluorocarbon uptake in a world ocean model 2. Sensitivity to surface thermohaline forcing and subsurface mixing parameterization, J. Geophys. Res., 102, 15 709–15 731, 1997. 1028
Enting, I., Wigley, T., and Heimann, M.: Future Emissions and Concentrations of Carbon Dioxide: Key Ocean/Atmosphere/Land Analyses, Tech. rep., CSIRO Division of Atmospheric Research, 1994. 1020
Fichefet, T. and Maqueda, M. M.: Sensitivity of a global sea ice model to the treatment of ice thermodynamics and dynamics, J. Geophys. Res., 102, 12 609–12 646, 1997. 1019
Gaspar, P., Gregorius, Y., and Lefevre, J.-M.: A simple eddy kinetic energy model for simulations of oceanic vertical mixing tests at Station Papa and Long-Term Upper Ocean Study Site, J. Geophys. Res., 95, 16 179–16 193, 1990. 1018

Gent, P. R. and McWilliams, J. C.: Isopycnal mixing in ocean circulation models, J. Phys. Oceanogr., 20, 150–155, 1990. 1028

Gent, P. R., Willebrand, J., McDougall, T. J., and McWilliams, J. C.: Parameterizing eddy-induced tracer transports in ocean circulation models, J. Phys. Oceanogr., 25, 463–474, 1995. 1028

GLOBALVIEW-CO_2: Cooperative Atmospheric Data Integration Project – Carbon Dioxide, CD-ROM, NOAA CMDL, Boulder, Colorado (Also available on Internet via anony mous FTP to ftp://ftp.cmdl.noaa.gov/ccg/co2/GLOBALVIEW/, Path: ccg/co2/GLOBALVIEW), 2003. 1020

Goose, H.: Modeling the large scale behaviour of the coupled ocean-sea ice system, PhD thesis, Université Catholique de Louvain, Louvain-la-Neuve, Belgium, 1997. 1018

Griffies, S. M., Boning, C., Bryan, F. O., Chassignet, E. P., Gerdes, R., Hasumi, H., Hirst, A., Treguier, A.-M., and Webb, D.: Developments in ocean climate modelling, Ocean Modelling, 2, 123–192, 2000. 1018

Hallberg, R. W. and Gnanadesikan, A.: An exploration of the role of transient eddies in determining the transport of a zonally reentrant current, J. Phys. Oceanogr., 31, 3312–3330, 2001. 1030

Hill, H., Hill, C., Follows, M., and Dutkiewicz, S.: Is there a computational advantage to offline tracer modeling at very high resolution?, Geophys. Res. Abstr., 6, EGU04-A-06348, 2004. 1017

Hirst, A. and McDougall, T. J.: Deep-water properties and surface buoyancy flux as simulated by a z-coordinate model including eddy-induced advection, J. Phys. Oceanogr., 26, 1320–1343, 1996. 1028

Holland, W. R.: The role of mesoscale eddies in the general circulation of the ocean: Numerical experiments using a wind-driven quasigeostrophic model, J. Phys. Oceanogr., 8, 363–392, 1978. 1013

Holland, W. R. and Lin, L. B.: On the origin of mesoscale eddies and their contribution to the general circulation of the ocean. I. A preliminary numerical experiment, J. Phys. Oceanogr., 5, 642–657, 1975a. 1013

Holland, W. R. and Lin, L. B.: On the origin of mesoscale eddies and their contribution to the general circulation of the ocean. II. A parameter study, J. Phys. Oceanogr., 5, 658–669, 1975b. 1013

Holton, J.: An advective model for two-dimensional transport of stratoshperic trace species, J. Geophys. Res., 86, 11 989–11 994, 1981. 1029

Ito, T., Marshall, J., and Follows, M.: What controls the uptake of transient tracers in the Southern Ocean?, Global Biogeochem. Cycles, 18, GB2021, doi:10.1029/2003GB002103, 2004. 1015
Jackett, D. R. and McDougall, T. J.: Minimal adjustment of hydrographic profiles to achieve static stability, J. Atmos. Oceanic Technol., 12, 381–389, 1995. 1017
Jakobsson, M., Cherkis, N., Woodward, J., Coakley, B., and Macnab, R.: A new grid of Arctic bathymetry: A significant resource for scientists and mapmakers, Eos Trans AGU, 81(9), p. 89, 93, 96, 2000. 1018
Joos, F., Orr, J. C., and Siegenthaler, U.: Ocean carbon transport in a box-diffusion versus a general circulation model, J. Geophys. Res., 102, 12 367–12 388, 1997. 1021
Kalnay, E., Kanamitsu, M., Kistler, R., Collins, W., Deaven, D., Gandin, L., Iredell, M., Saha, S., White, G., Woollen, J., Zhu, Y., Chelliah, M., Ebisuzaki, W., Higgins, W., Janowiak, J., Mo, K. C., Ropelewski, C., Wang, J., Leetma, A., Reynolds, R., Jenne, R., and Joseph, D.: The NCEP/NCAR 40-year reanalysis project, Bull. Am. Meteor. Soc., 77, 437–471, 1996. 1018
Key, R. M., Lee, C. L. S. K., Wanninkhof, R., Bullister, J., Feely, R. A., Millero, F. J., Mordy, C., and Peng, T.-H.: A Global Ocean Carbon Climatology: Results from Global Data Analysis Project (GLODAP, Global Biogeochem. Cycles, 18, GB4031, doi:10.1029/2004GB002247, 2004. 1017, 1025, 1026, 1027, 1044
Levitus, S., Boyer, T., Conkright, M., O'Brian, T., Antonov, J., Stephens, C., Stathopolos, L., Johnson, D., and Gelfeld, R.: World Ocean Database 1998, Tech. rep., NOAA Atlas NESDID18, 1998. 1018
Lévy, M., Klein, P., and Treguier, A.: Impacts of sub-mesoscale dynamics on phytoplankton production and subduction, J. Mar. Res., 59, 535–565, 2001. 1018
Lythe, M. and Vaughan, D.: BEDMAP: a new ice thickness and subglacial topograpic model of Antarctica, J. Geophys. Res., 106, 11 335–11 351, 2001. 1018
Madec, G. and Imbard, M.: A global ocean mesh to overcome the North Pole singularity, Clim. Dyn., 12, 381–388, 1996. 1017
Madec, G., Delecluse, P., Imbard, M., and Lévy, C.: OPA version 8.0, Ocean General Circulation Model, Reference Manual, Note of the IPSL Modelling Pole 11, IPSL, 1998. 1017
Marshall, J. and Radko, T.: Residual-mean solutions for the Antarctic Circumpolar Current and its associated overturning circulation, J. Phys. Oceanogr., 33, 2341–2354, 2003. 1014
Marshall, J., Jones, H., Karsten, R., and Wardle, R.: Can Eddies Set Ocean Stratification?, J. Phys. Oceanogr., 32, 26-38, 2002. 1014, 1028

Marshall, J. C. and Nurser, A. J. G.: Fluid dynamics of the oceanic thermocline ventilation, J. Phys. Oceanogr., 22, 583–595, 1992. 1030
Marti, O., Madec, G., and Delecluse, P.: Comment on "Net diffusivity in ocean general circulation models with non uniform grids" by F. L. Yin and I. Y. Fung, J. Geophys. Res., 97, 12 763–12 766, 1992. 1018
Matear, R. J.: Effects of numerical advection schemes and eddy parameterizations on ocean ventilation and oceanic anthropogenic CO2 uptake, Ocean Modelling, 3, 217–248, 2001. 1013
Matsumoto, K., Sarmiento, J. L., Key, R. M., Aumont, O., Bullister, J. L., Caldeira, K., Campin, J.-M., Doney, S. C., Drange, H., Dutay, J.-C., Follows, M., Gao, Y., Gnanadesikan, A., Gruber, N., Ishida, A., Joos, F., Lindsay, K., Maier-Reimer, E., Marshall, J. C., Matear, R. J., Monfray, P., Mouchet, A., Najjar, R., Plattner, G.-K., Schlitzer, R., Slater, R., Swathi, P. S., Totterdell, I. J., Weirig, M.-F., Yamanaka, Y., Yool, A., and Orr, J. C.: Evaluation of ocean carbon cycle models with data-based metrics, Geophys. Res. Lett., 31, L07303, doi:10.1029/2003GL018970, 2004. 1013
McDougall, T. J.: Neutral surfaces, J. Phys. Oceanogr., 17, 1950–1964, 1987. 1029
McIntosh, P. C. and McDougall, T. J.: Isopycnal averaging and the residual mean circulation, J. Phys. Oceanogr., 26, 1655-1660, 1996. 1029
Orr, J. C., Monfray, P., Maier-Reimer, E., Mikolajewicz, U., Palmer, J., Taylor, N. K., Toggweiler, J. R., Sarmiento, J. L., Quéré, C. L., Gruber, N., Sabine, C. L., Key, R. M., and Boutin, J.: Estimates of anthropogenic carbon uptake from four three-dimensionsal global ocean models, Global Biogeochem. Cycles, 15, 43–60, 2001. 1013, 1021
Price, J. F.: Ocean Circulation and Climate: Observing and Modelling the Global Ocean, chap. Subduction, pp. 357–371, Academic Press, 2001. 1031
Robbins, P. E., Price, J. F., Owens, W., and Jenkins, W.: On the importance of lateral diffusion for the ventilation of the lower thermocline in the Subtropical North Atlantic, J. Phys. Oceanogr., 30, 67–89, 2000. 1031
Sabine, C. L., Feely, R. A., Gruber, N., Key, R. M., Lee, K., Bullister, J. L., Wanninkhof, R., Wong, C. S., Wallace, D. W. R., Tilbrook, B., Millero, F. J., Peng, T.-H., Kozyr, A., Ono, T., and Rios, A.: The ocean sink for anthropogenic CO_2, Science, 305, 367–370, 2004. 1027, 1044
Sarmiento, J. L. and Gruber, N.: Ocean Biogeochemical Dynamics, Princeton University Press, 2006. 1015
Sarmiento, J. L., Orr, J. C., and Siegenthaler, U.: A perturbation simulation of CO_2 uptake in

an ocean general circulation model, J. Geophys. Res., 97, 3621–3645, 1992. 1016, 1021, 1034
Sarmiento, J. L., Le Quéré, C., and Pacala, S. W.: Limiting future atmospheric carbon dioxide, Global Biogeochem. Cycles, 9, 121–137, 1995. 1034
Sasai, Y., Ishida, A., Yamanaka, Y., and Sasaki, H.: Chlorofluorocarbons in a global ocean eddy-resolving OGCM: Pathway and formation of Antarctic Bottom Water, Geophys. Res. Lett., 31, L12305, doi:10.1029/2004GL019895, 2004. 1013, 1026, 1044, 1054
Sen Gupta, A. and England, M.: Evaluation of interior circulation in a high resolution global ocean model, Part I: Deep and Bottom Waters, J. Phys. Oceanogr., 34, 2592–2614, 2004. 1017
Siegenthaler, U. and Joos, F.: Use of a simple model for studying oceanic tracer distributions and the global carbon cycle, Tellus, 44B, 186–207, 1992. 1016, 1021, 1034
Smith, W. H. F. and Sandwell, D. T.: Global seafloor topography from satellite altimetry and ship depth soundings, Science, 277, 1957–1962, 1997. 1018
Smolarkiewicz, K. P.: The multidimensional Crowley advection scheme, Mon. Weather Rev., 110, 1968–1983, 1982. 1019
Smolarkiewicz, K. P.: A simple positive advection scheme with small implicit diffusion, Mon. Weather Rev., 111, 479–486, 1983. 1019
Smolarkiewicz, K. P. and Clark, T. L.: The multidimensional positive definite advection transport algorithm: further development and applications, J. Comp. Phys., 67, 396–438, 1986. 1019
Steele, M., Morley, R., and Ermold, W.: PHC: A global ocean hydrography with a high quality Arctic Ocean, J. Climate, 14, 2079–2087, 2001. 1018
Thompson, S. R., Stevens, D. P., and Döös, K.: The importance of interocean exchange south of Africa in a numerical model, J. Geophys. Res., 102, 3303-3315, 1997. 1014
Toggweiler, J. R., Dixon, K., and Bryan, K.: Simulations of radiocarbon in a coarse resolution world ocean model 1. Steady state prebomb distributions, J. Geophys. Res., 94, 8217–8242, 1989a. 1021, 1022
Toggweiler, J. R., Dixon, K., and Bryan, K.: Simulations of radiocarbon in a coarse resolution world ocean model 2. Distributions of bomb-produced carbon 14, J. Geophys. Res., 94, 8243–8264, 1989b. 1021
Trenberth, K. E., Olson, J. G., and Large, W. G.: A global ocean wind stress climatology based on ECMWF analyses, Report NCAR/TN-338 +STR, National Center for Atmos. Res., Boulder, Colorado, 93 pp., 1989. 1018

Vallis, G. K.: Thermocline theories and WOCE: A mutual challenge, International International WOCE Newsletter, 39, WOCE International Project Office, Southampton, United Kingdom, 3-5, 2000. 1014

Walker, S., Weiss, R., and Salameh, P.: Reconstructed histories of the annual mean atmospheric mole fractions for halocarbons CFC-11, CFC-12, CFC-113, and carbon tetrachloride, J. Geophys. Res., 105, 14 285–14 296, 2000. 1019

Wallace, D. and Lazier, J.: Anthropogenic chlorofluoromethanes in newly formed Labrador Sea water, Nature, 332, 61–63, 1988. 1019

Wanninkhof, R.: Relationship between wind speed and gas exchange over the ocean, J. Geophys. Res., 97, 7373–7382, 1992. 1020

Warner, M. and Weiss, R.: Chorofluoromethanes in south atlantic antarctic intermediate water, Deep Sea Res., 39, 2053–2075, 1992. 1026

Watson, A. J. and Orr, J. C.: Carbon dioxide fluxes in the global ocean, in: Ocean Biogeochemistry: the Role of the Ocean Carbon Cycle in Global Change (a JGOFS Synthesis), edited by: Fasham, M., Field, J., Platt, T., and Zeitzschel, B., chap. 5, pp. 123–141, Springer, Berlin, 2003. 1013

Willey, D. A., Fine, R. A., Sonnerup, R. E., Bullister, J. L., Smethie Jr., W. M., and Warner, M. J.: Global oceanic chlorofluorocarbon inventory, Geophys. Res. Lett., 31, L01303, doi:10.1029/2003GL018816, 2004. 1026, 1044

Xie, P. and Arkin, P. A.: Analyses of global monthly precipitation using gauge observations, satellite estimates and numerical model predictions, J. Clim., 9, 840–858, 1996. 1018

Table 1. Changes in integrated global- and basin-scale, air-to-sea tracer fluxes when moving from the non-eddying to the eddying model.

	CFC-11	CO_2	$\Delta^{14}C$
Atlantic	–34%	–21%	–4%
Pacific	–10%	–12%	–4%
Indian	–23%	–24%	–6%
South of 20° S	–28%	–25%	–7%
South of 50° S	–19%	–23%	–6%
Global	–22%	–18%	–5%

OSD

3, 1011–1063, 2006

Table 2. Changes in integrated basin-scale tracer inventories when moving from the non-eddying to the eddying model.

	CFC-11	CO_2	$\Delta^{14}C$
Atlantic	–23%	–18%	–6%
Pacific	–11%	–14%	–2%
Indian	–37%	–25%	–7%
South of 20° S	–31%	–26%	–9%
South of 50° S	–44%	–35%	–14%

OSD
3, 1011–1063, 2006

Table 3. Global inventories of the three transient tracers from the data-based estimates (Key et al., 2004; Willey et al., 2004; Sabine et al., 2004) and as simulated by ORCA2, ORCA05, and the eddy resolving model from Sasai et al. (2004).

	CFC-11 (10^6 mol)	CO_2 (Pg C)	$\Delta^{14}C$ (10^{28} atoms ^{14}C)
ORCA2 (non-eddying)	648	120	3.07
ORCA05 (eddying)	506	98	2.94
GLODAP	544 (±81)	106 (±16)	3.13 (±0.47)
Willey et al. (2004)	550	–	–
Sasai et al. (2004)	510	–	–
Sabine et al. (2004)	–	106	–

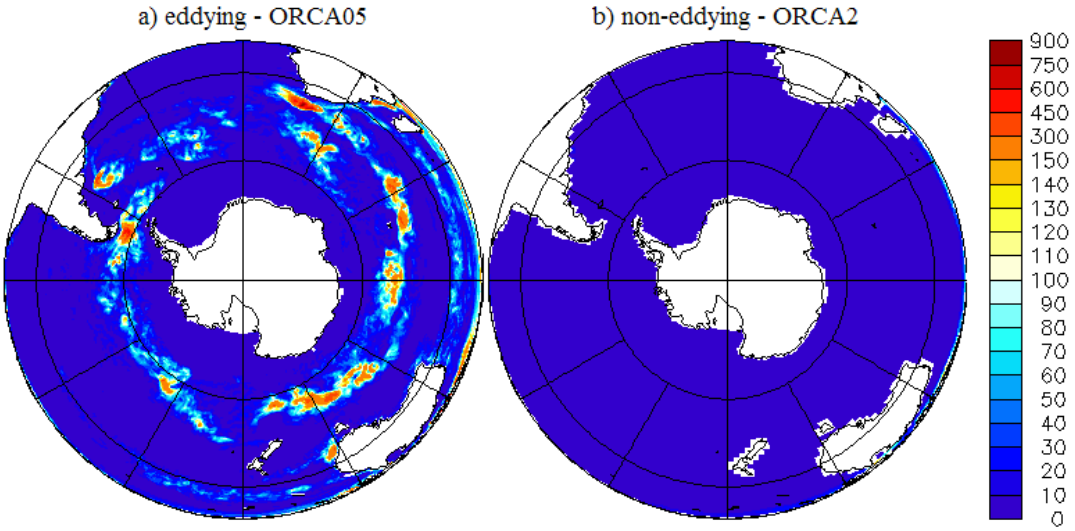

Fig. 1. Southern Hemisphere map of eddy kinetic energy (in $cm^2\,s^{-2}$) in the eddying and non-eddying simulations.

OSD
3, 1011–1063, 2006

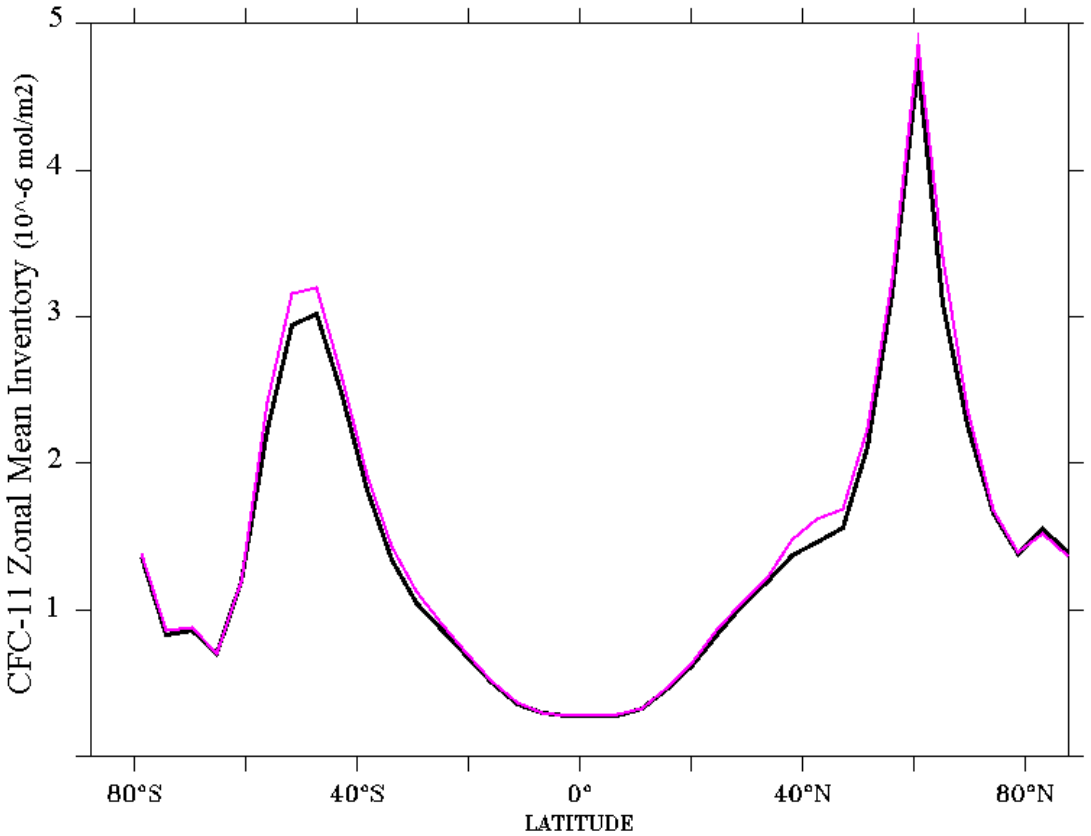

Fig. 2. Zonal mean inventory of CFC-11 at end of 1994, as given by an online (black) and an offline (purple) versions of the non-eddying model.

OSD
3, 1011–1063, 2006

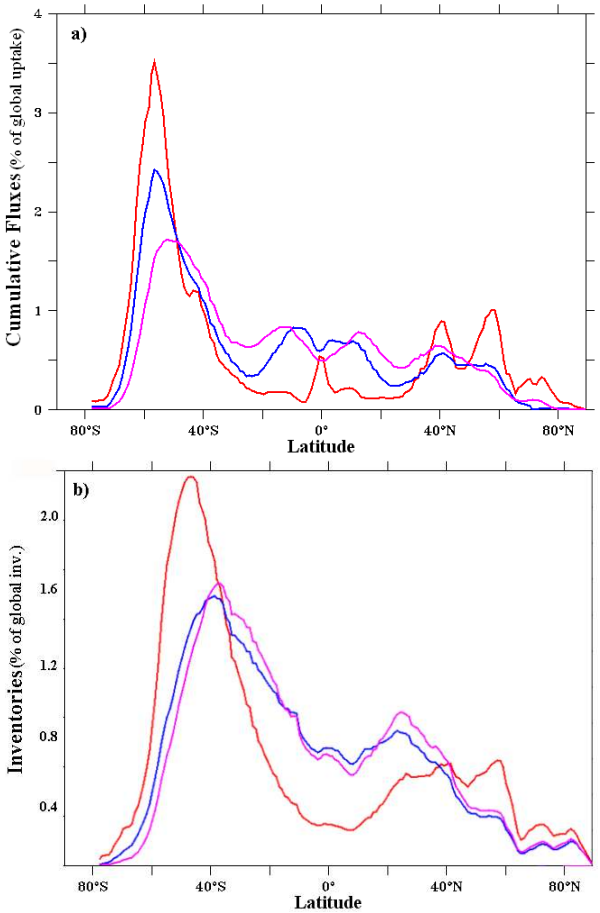

Fig. 3. Zonal integrals of the normalized **(a)** cumulative fluxes and **(b)** inventories of CFC-11 (red), anthropogenic CO_2 (blue) and bomb $\Delta^{14}C$ (purple) as simulated by ORCA2 at end of 1994. Cumulative fluxes and inventories were normalized by dividing by the total global uptake.

OSD
3, 1011–1063, 2006

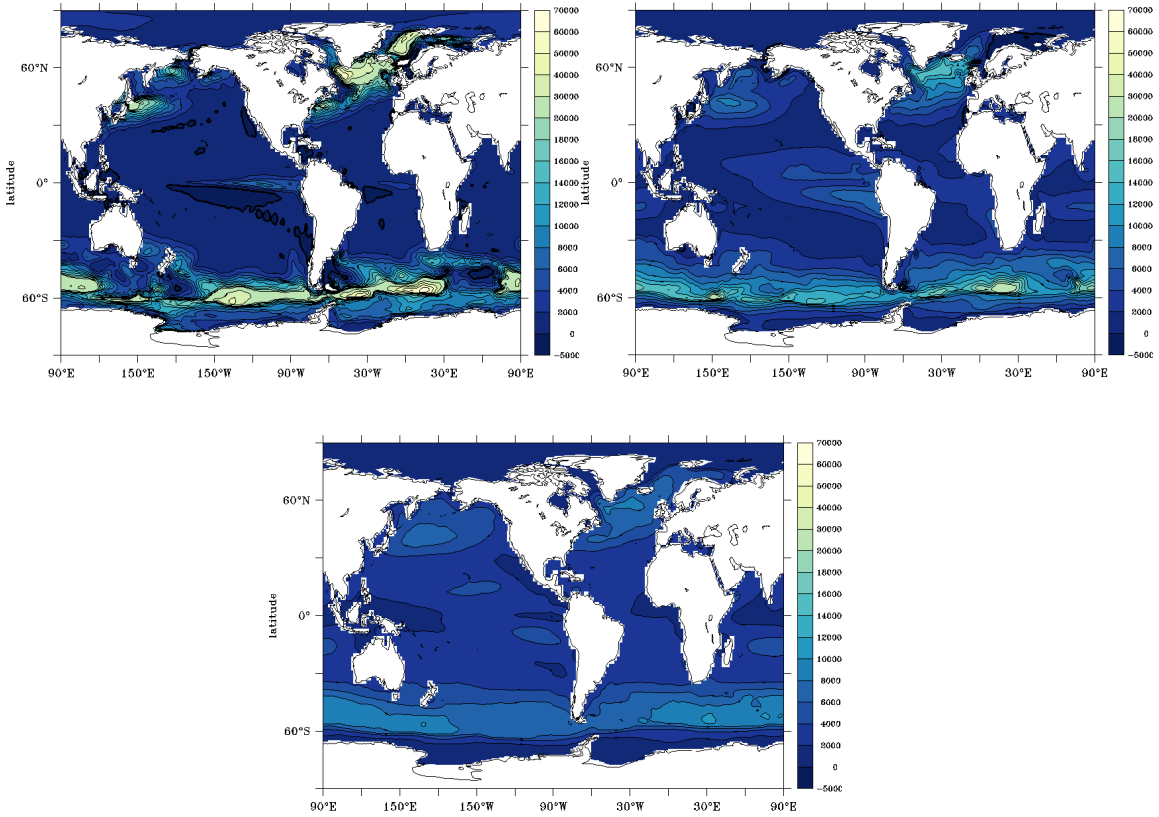

Fig. 4. Normalized cumulative fluxes obtained by dividing by the global ocean mean concentration for (upper left panel) CFC-11, (upper right panel) anthropogenic CO_2 and (lower panel) bomb $\Delta^{14}C$ at end of year 1994.

OSD
3, 1011–1063, 2006

EGU

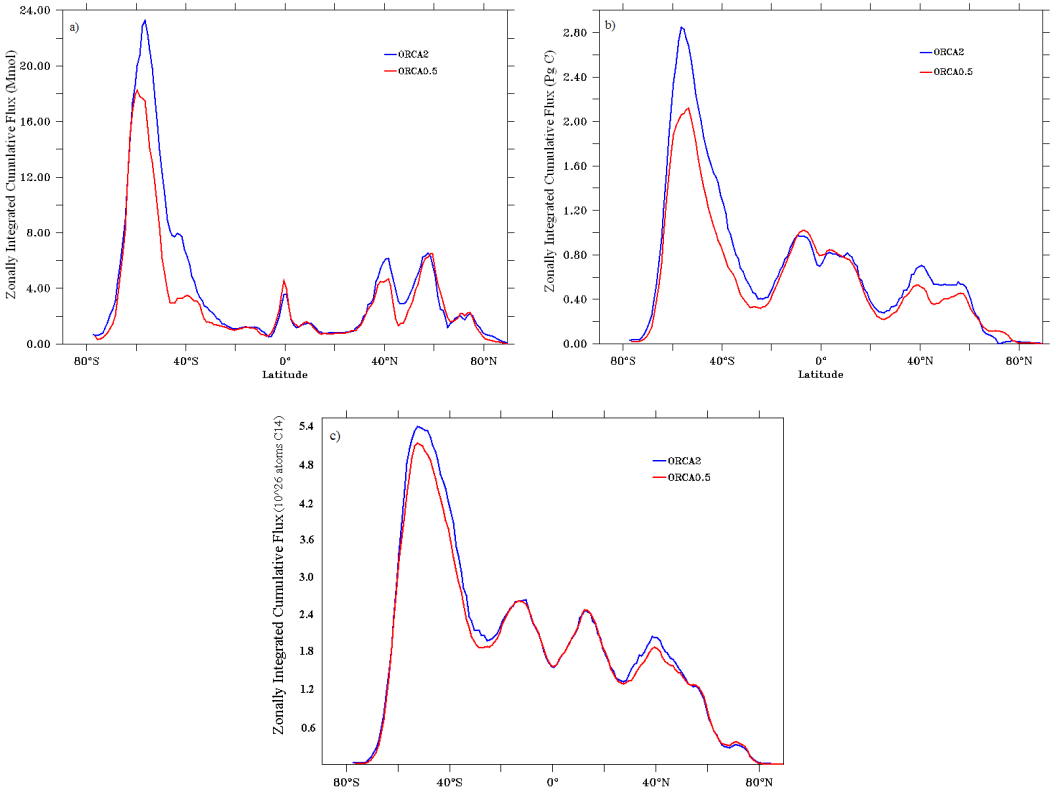

Fig. 5. Cumulative fluxes at the end of 1994 for **(a)** CFC-11, **(b)** anthropogenic CO_2 and **(c)** bomb $\Delta^{14}C$ as simulated by the non-eddying (blue) and the eddying models (red).

OSD
3, 1011–1063, 2006

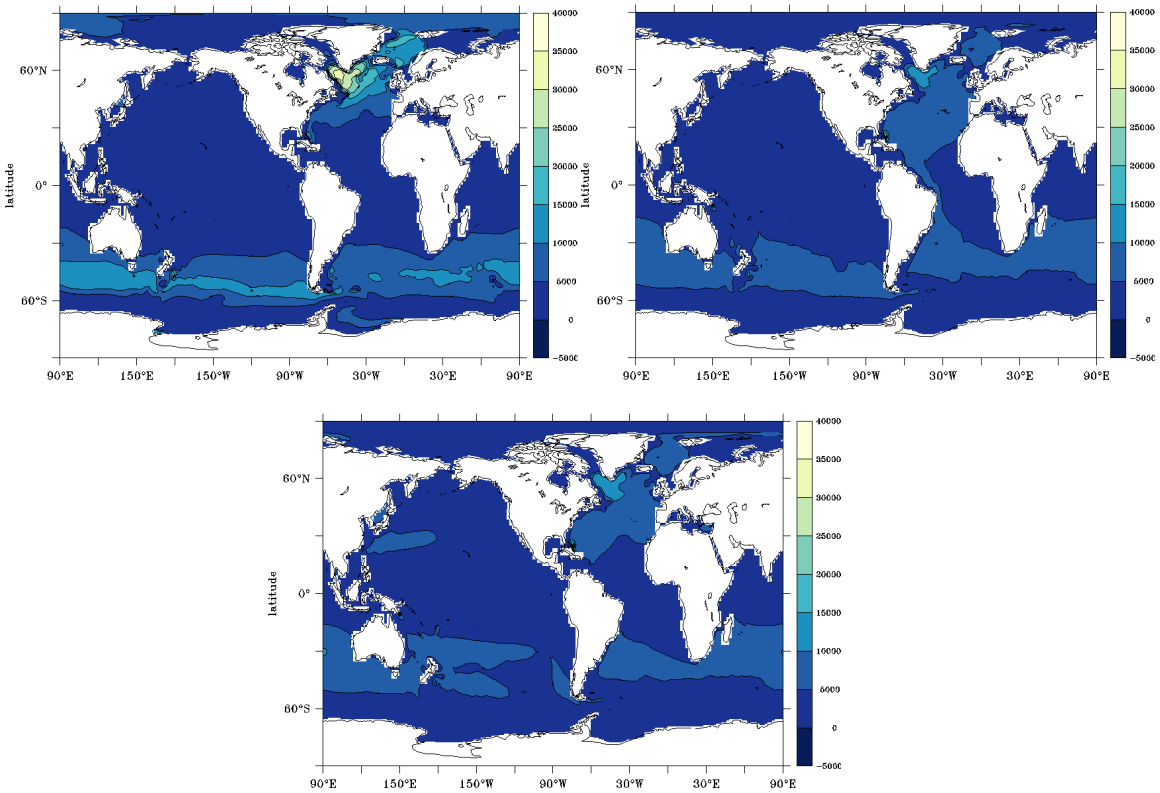

Fig. 6. Normalized inventories, obtained by dividing by the mean concentration for (upper left panel) CFC-11, (upper right panel) anthropogenic CO_2, and (lower panel) bomb $\Delta^{14}C$ at end of year 1994.

OSD
3, 1011–1063, 2006

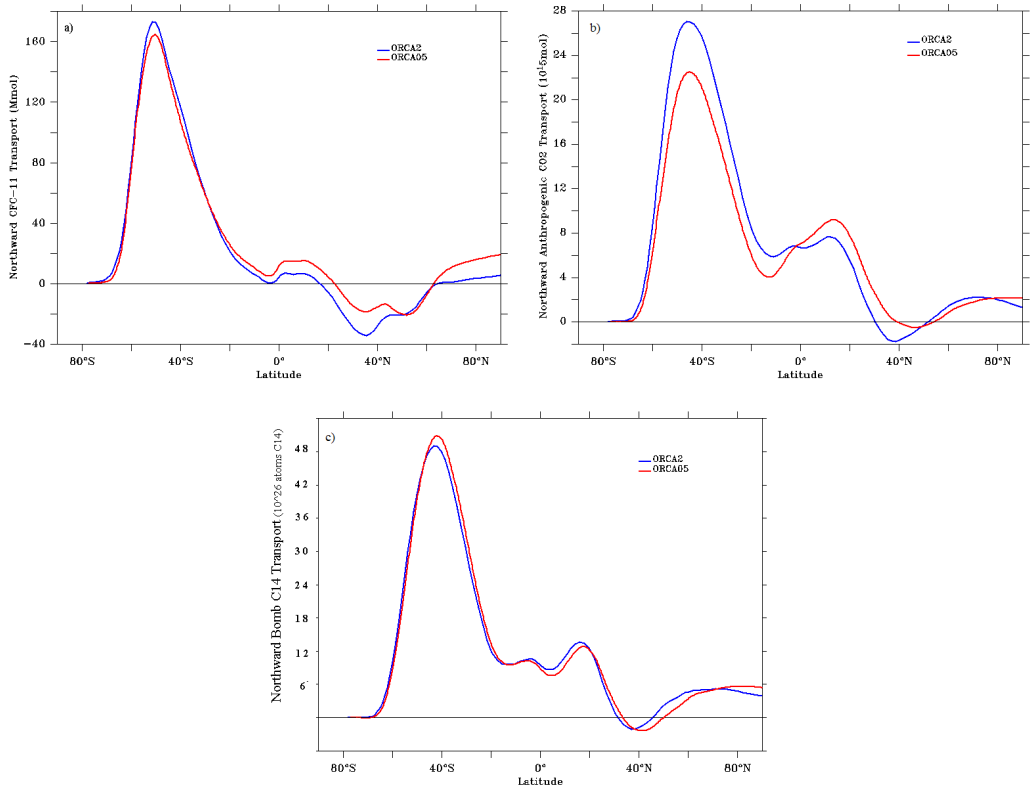

Fig. 7. Northward transport of **(a)** CFC-11, **(b)** anthropogenic CO_2 and **(c)** bomb $\Delta^{14}C$ as simulated by the non-eddying (blue) and the eddying (red) model at end of year 1994.

OSD
3, 1011–1063, 2006

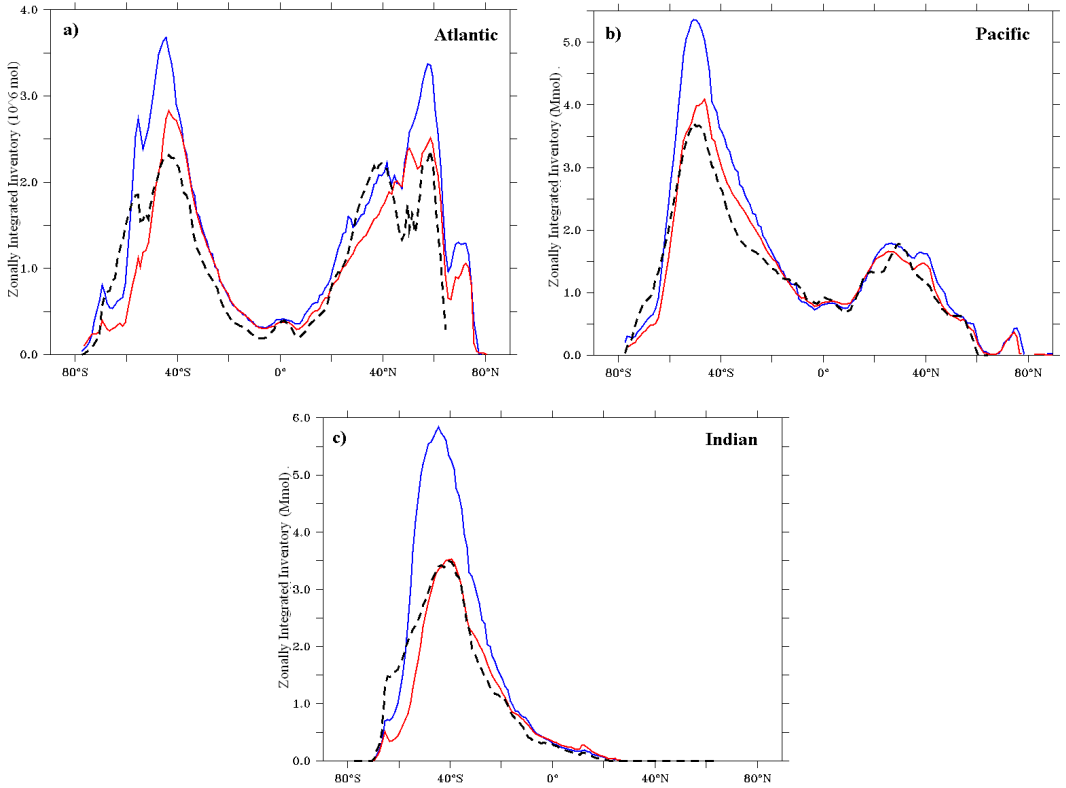

Fig. 8. Zonally integrated basin-scale inventories of CFC-11 for the **(a)** Atlantic, **(b)** Pacific, and **(c)** Indian Oceans as observed (black dashes, GLODAP) and as simulated by the eddying (red) and the non-eddying (blue) model at end of year 1994.

OSD
3, 1011–1063, 2006

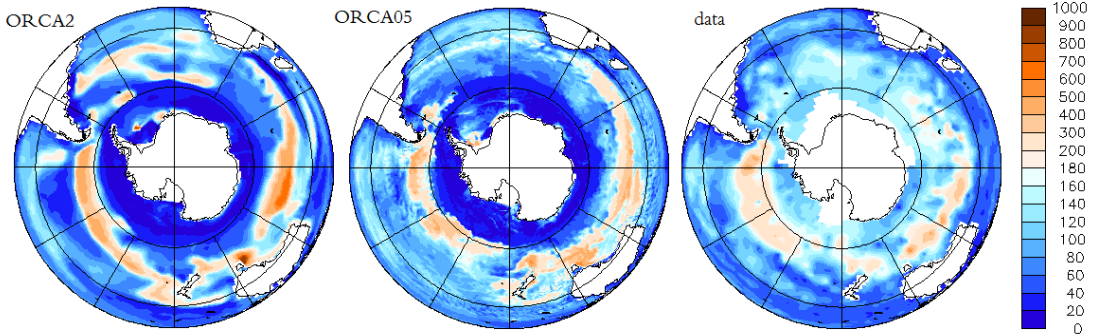

Fig. 9. Mixed layer depth (m) in the Southern Hemisphere (September) as simulated by the non-eddying and the eddying model and from an observational climatology (de Boyer Montégut et al., 2004).

OSD
3, 1011–1063, 2006

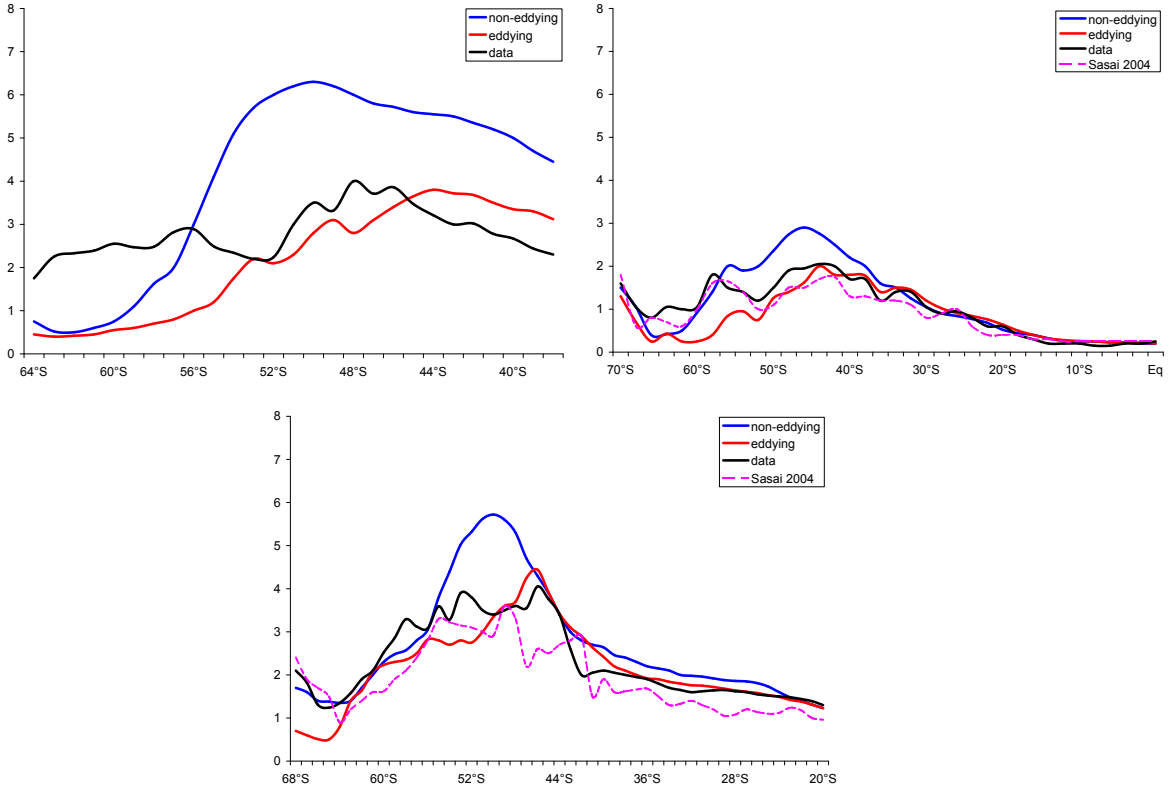

Fig. 10. CFC-11 inventories along (upper left panel) the WOCE I9S section on 115° E in the Indian sector of the Southern Ocean, (upper right panel) the AJAX section along 0° E in the South Atlantic, and (lower panel) the WOCE P15S section on 170° W in the South Pacific, as observed (black) and as simulated by the non-eddying (blue) and the eddying (red) model. The purple curves show Sasai et al. (2004) inventories.

OSD
3, 1011–1063, 2006

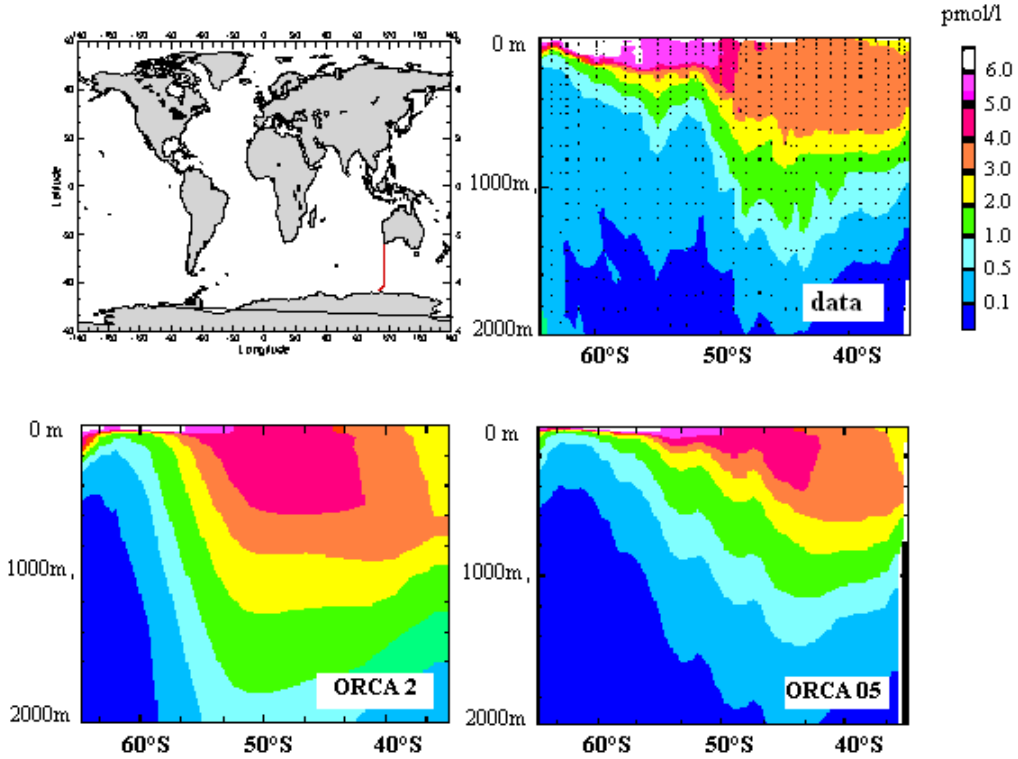

Fig. 11. CFC-11 concentration (in pmol l^{-1}) along the WOCE I9S section (115° E, 1994–1995) as observed and simulated by the non-eddying (ORCA2) and the eddying (ORCA05) model.

OSD
3, 1011–1063, 2006

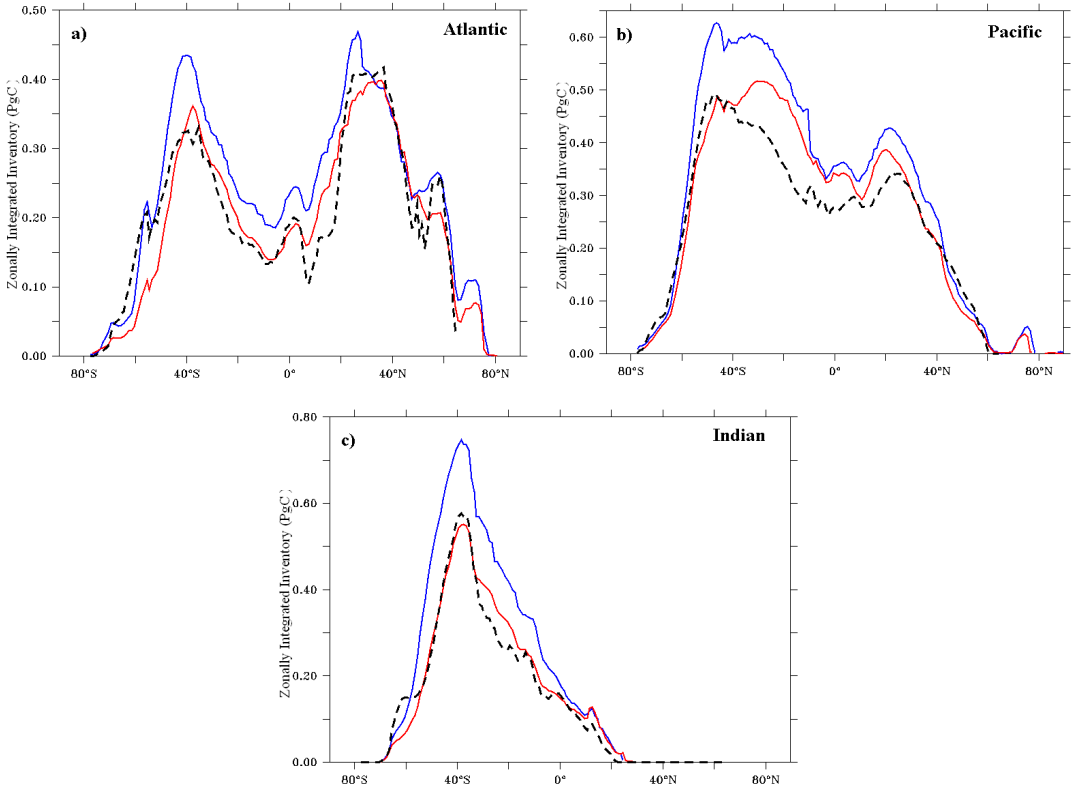

Fig. 12. Zonally basin-integrated inventories of anthropogenic CO_2 in **(a)** Atlantic, **(b)** Pacific, and **(c)** Indian Oceans, as observed (black dashes, GLODAP) and simulated by the eddying (red) and the non-eddying (blue) model at end of year 1994.

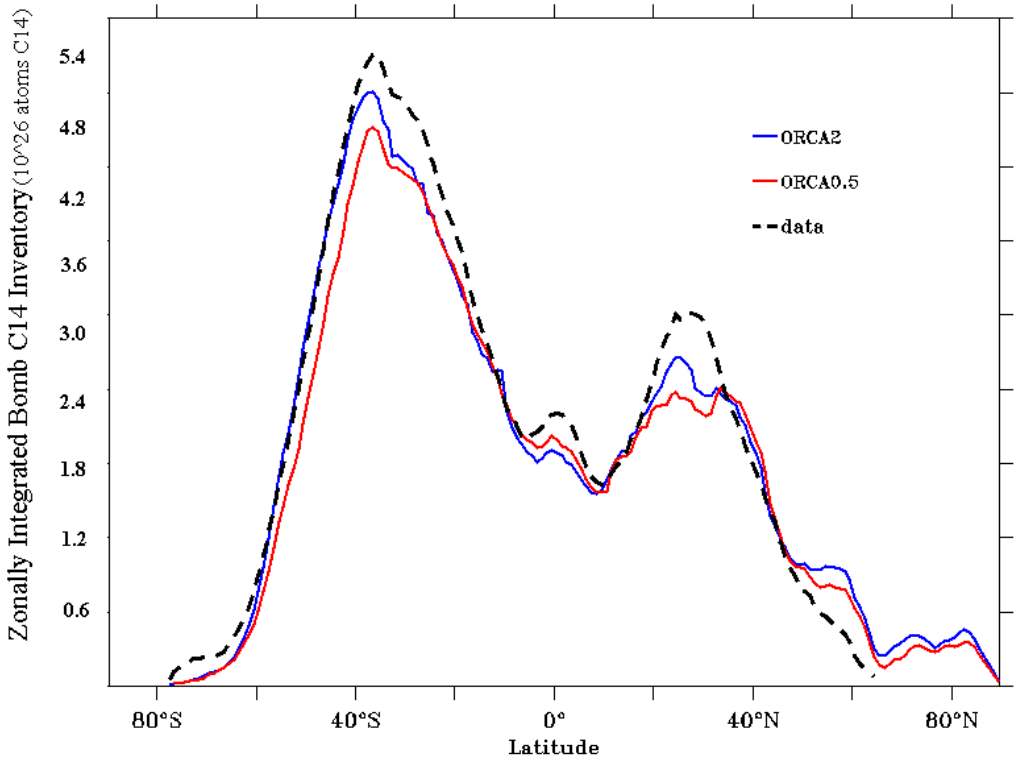

Fig. 13. Zonal integrals of inventories of bomb $\Delta^{14}C$ as observed (black dashes, GLODAP) and as simulated by the eddying (red) and the non-eddying (blue) model at end of year 1994.

OSD
3, 1011–1063, 2006

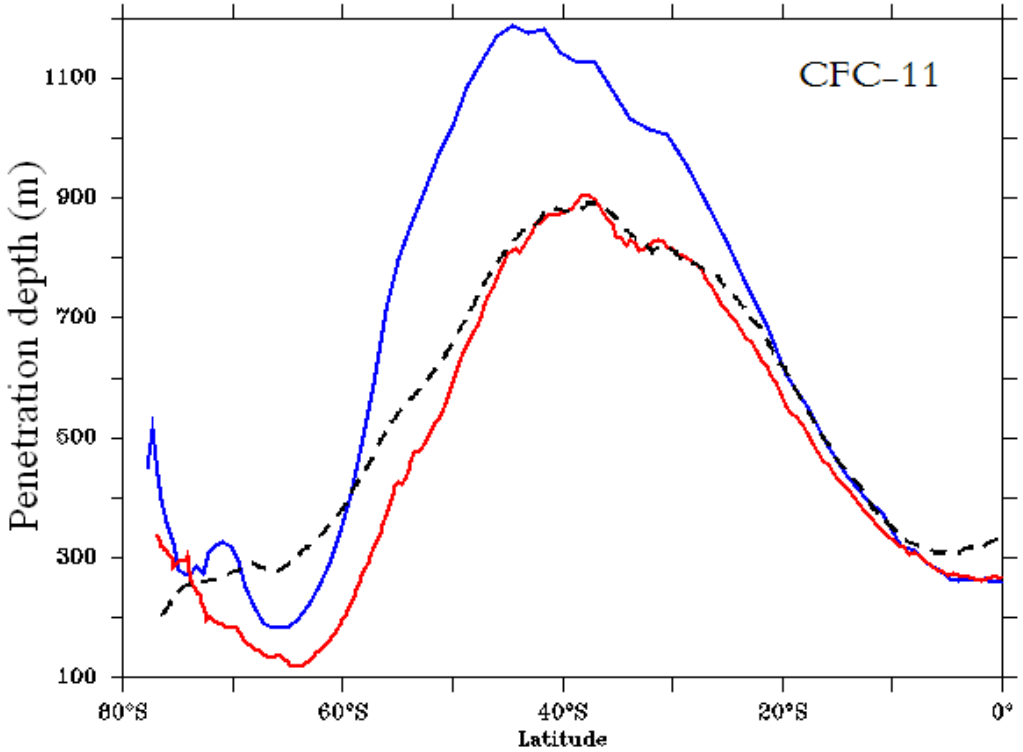

Fig. 14. Zonal mean of CFC-11 penetration depth (in m) as observed (black dashes, GLODAP) and as simulated by the eddying (red) and the non-eddying (blue) model over the Southern Hemisphere. The penetration depth of a tracer is defined as the tracer inventory divided by its surface concentration.

OSD
3, 1011–1063, 2006

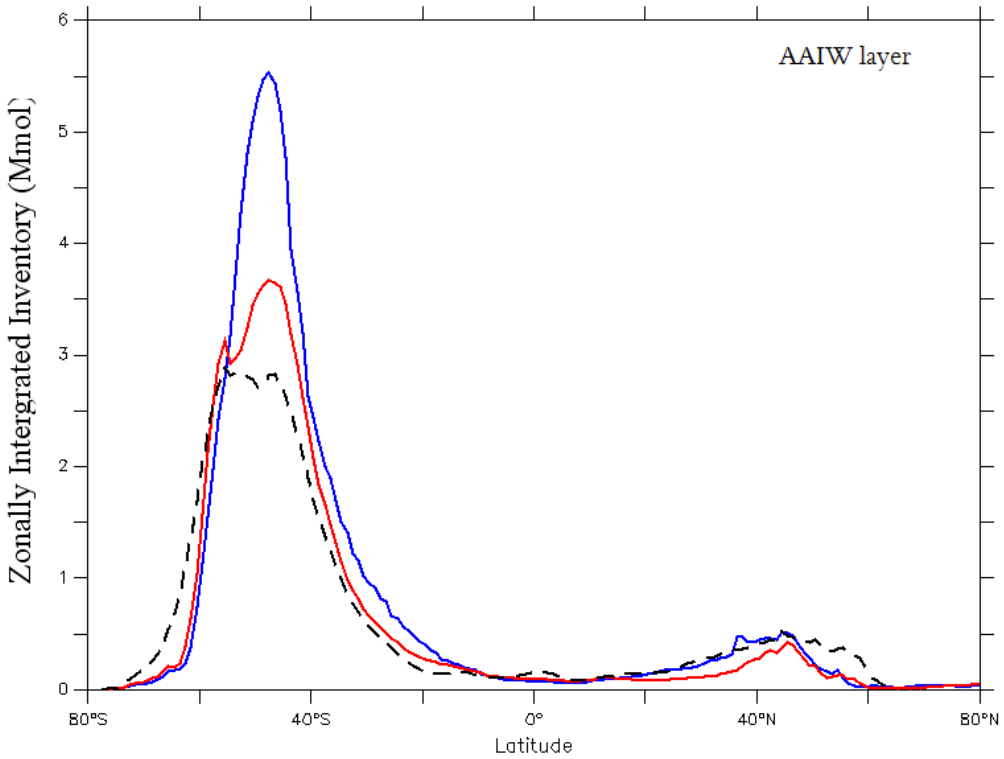

Fig. 15. Zonal integral of CFC-11 inventory (10^6 mol) in the AAIW, defined as the 27.0–27.4 σ_0 layer, as observed (black dashes, GLODAP) and as simulated by the non-eddying (blue) and the eddying (red) model.

OSD
3, 1011–1063, 2006

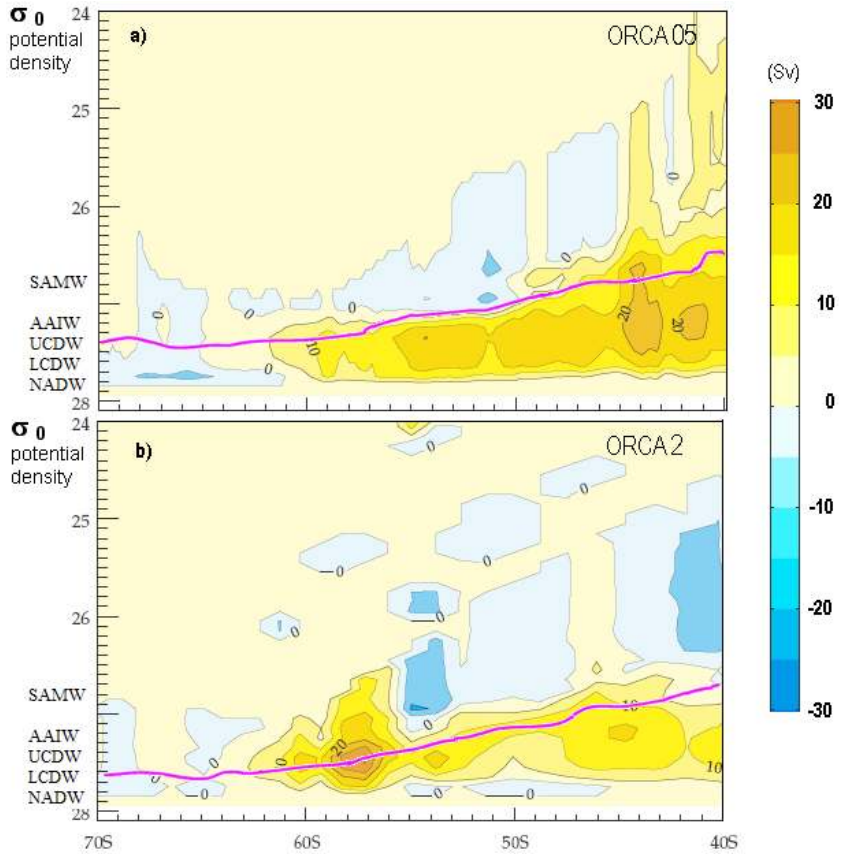

Fig. 16. The isopycnal transport streamfunction (in Sv) plotted in σ_0 coordinate for the eddying (ORCA05) and the non-eddying (ORCA2) model for the region south of 40° S. The contour interval is 5 Sv. The purple line indicates the position of the annual maximum mixed layer depth (m).

OSD
3, 1011–1063, 2006

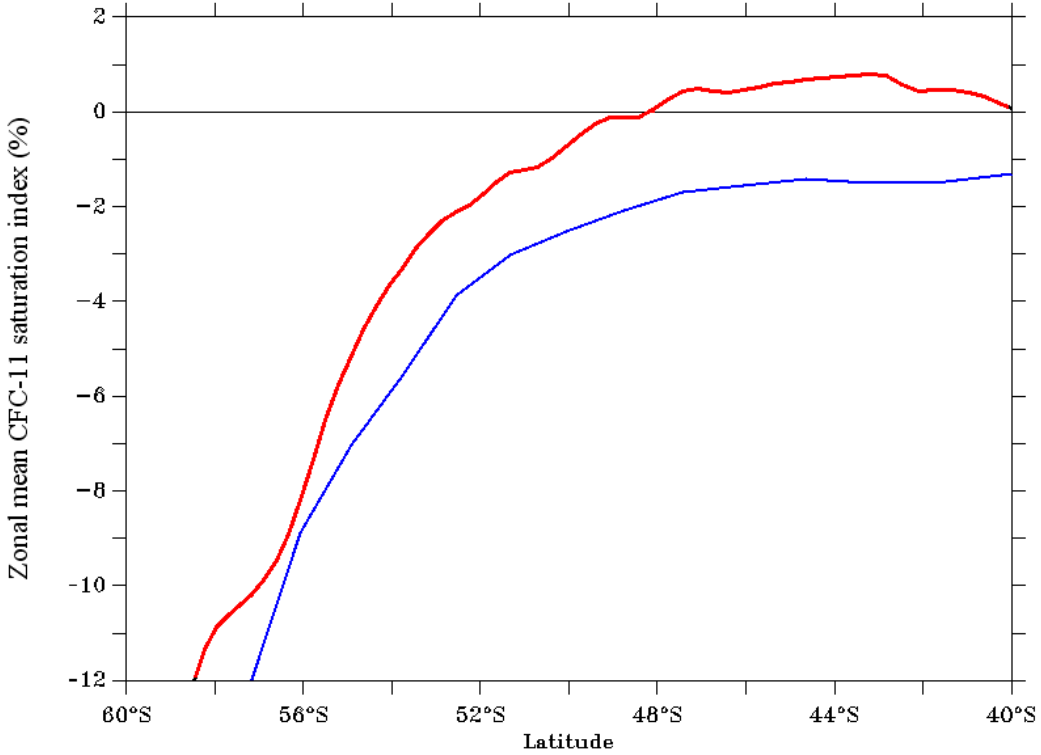

Fig. 17. Zonal mean of the CFC-11 saturation index in the Atlantic between 60° S and 40° S for the non-eddying (blue) and the eddying (red) model.

OSD

3, 1011–1063, 2006

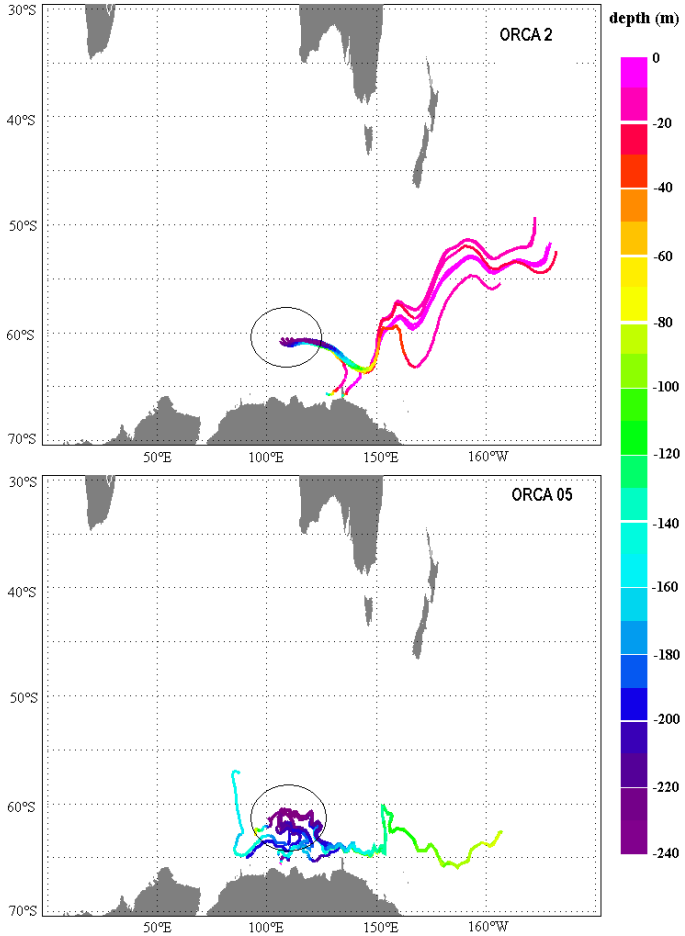

Fig. 18. Four-year trajectories of 10 particles launched from 250 m at 60° S, between 110° E and 120° E. Colors represent the depth of the particles.

OSD
3, 1011–1063, 2006

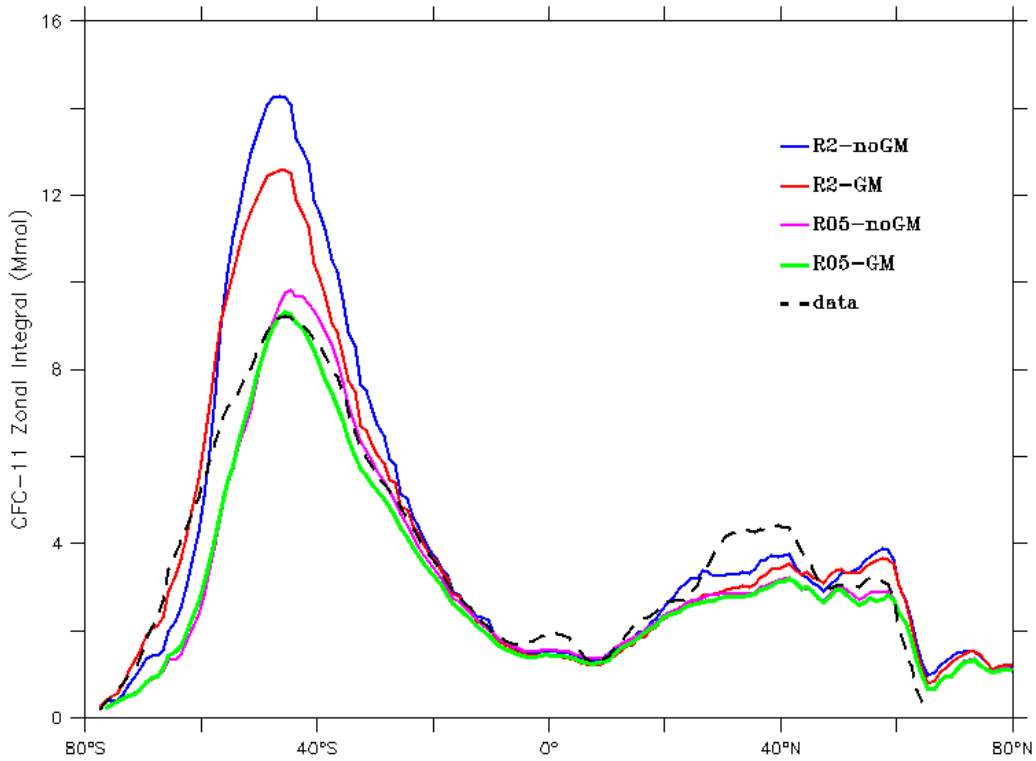

Fig. 19. Zonally integrated inventories of CFC-11 in 1994 as observed (black dashes, GLODAP) and as simulated by the non-eddying model with GM (red) and without GM (blue) as well as by the eddying model with GM (green) and without GM (purple).

OSD

3, 1011–1063, 2006